Combining multi-phase flow and pathway-specific reactive transport modeling to investigate the impact of water table fluctuations on dichloromethane biodegradation

Maria Prieto-Espinoza, Raphaël Di Chiara Roupert, Emilie Muller, Stéphane Vuilleumier, Gwenaël Imfeld, Sylvain Weill

Combining multi-phase flow and pathway-specific reactive transport modeling to investigate the impact of water table fluctuations on dichloromethane biodegradation

Maria Prieto-Espinoza[1,+,*], Raphaël Di Chiara Roupert[1], Emilie E. L. Muller[2], Stéphane Vuilleumier[2], Gwenaël Imfeld[1], Sylvain Weill[1]

[1] Université de Strasbourg, CNRS/EOST, ITES UMR 7063, Institut Terre et Environnement de Strasbourg, Strasbourg, France

[2] Université de Strasbourg, CNRS, GMGM UMR 7156, Génétique Moléculaire, Génomique, Microbiologie, Strasbourg, France

*Corresponding author: Maria Prieto-Espinoza

Email address: prietoespinoza.maria@gmail.com

[+]Present address: Aix-Marseille Université, CNRS UMR 7376, Laboratoire Chimie Environnement, Marseille, France

Manuscript for Advances in Water Resources

Abstract

Water table fluctuations play a significant role in the redistribution of chemical species, microorganisms and organic pollutants in aquifers by creating favorable zones for reactive processes. This in turn is expected to affect the extent and pathways of biodegradation of halogenated contaminants such as dichloromethane (DCM). Here, a multi-phase flow reactive transport model (RTM) was developed to identify the main drivers of DCM biodegradation in aquifers under steady-state and transient conditions. The RTM includes a description of multi-phase flow, redox conditions, four characteristic bacterial populations and stable isotopologues (i.e., $^{13}C/^{12}C$ and $^{37}Cl/^{35}Cl$) of DCM according to pathway-specific reactions. Dissolved organic carbon (DOC) was also included as a carbon source for non-DCM degrading populations yielding a more realistic heterotrophic groundwater microbial community. Numerical simulations of eight model scenarios were compared with experimental results from laboratory aquifers. Key biogeochemical processes involved in DCM biodegradation were captured, particularly across the capillary fringe. Only model scenarios of DCM degradation by multiple bacterial metabolisms were able to reproduce the dynamics observed in the laboratory aquifers. The observed and computed enrichment of ^{13}C and ^{37}Cl isotopes over time confirmed enhanced DCM biodegradation during water table fluctuations and highlighted interactions between different bacterial metabolisms. In particular, our RTM suggested that heterotrophic groundwater bacteria played a key role in regulating O_2-depletion and redox conditions across fluctuation zones during parallel DOC mineralization. The produced CO_2 favored metabolic activity of anaerobic DCM degraders requiring CO_2 for their specific fermentative pathways. This study underscores the added value of integrating multi-phase flow, stable isotopes and distinct bacterial populations to understand natural attenuation of DCM in contaminated groundwater.

Keywords: multi-phase flow, reactive transport modeling, CSIA, bacterial populations, DCM, water table fluctuations

Highlights

- A multi-phase flow reactive transport model was developed to examine DCM biodegradation
- The model captured biogeochemical processes during DCM biodegradation under steady-state and transient conditions
- Heterotrophic groundwater bacteria favored anaerobic DCM degraders requiring CO_2
- DCM degradation by multiple bacterial populations reproduced the DCM dynamics observed in laboratory aquifers

Graphical abstract

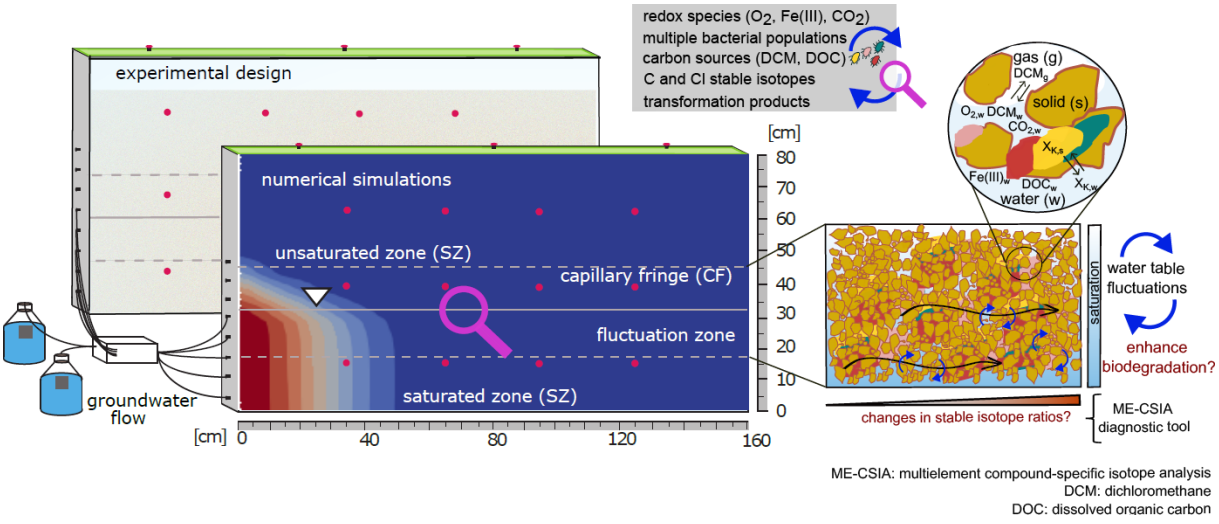

1. Introduction

Reactive transport in aquifers involves a complex interplay between multi-phase flow, transport of elements and pollutants, chemical reactions and microbial activities (Carrera et al., 2022; Meile & Scheibe, 2019). Water table fluctuations can affect the transfer of volatile organic pollutants (McCarthy & Johnson, 1993; Werner & Höhener, 2002), distribution of redox species (Haberer et al., 2012; Rezanezhad et al., 2014; Seybold et al., 2002) and composition of microbial communities (Jost et al., 2015a; Pronk et al., 2020; Rühle et al., 2015). These biogeochemical variations can support reactive processes in aquifers that may alter the degradation extent and pathways of common organic pollutants (Prieto-Espinoza et al., 2021). However, variations of biogeochemical conditions and pollutant transformation during water table fluctuations remain difficult to predict quantitatively under field conditions, restricting the accuracy of long-term monitoring of contaminated sites (Zhang & Furman, 2021).

Natural attenuation in contaminated aquifers largely relies on the ability of microorganisms to oxidize organic pollutants while reducing available electron acceptors (e.g., O_2, NO_3^-, Fe^{3+}) (Meckenstock et al., 2015). Monitoring hydrochemical conditions including contaminant concentrations and contaminant-degrading bacterial populations may help to identify active contaminant transformation processes and prevailing degradation pathways in aquifers. The extent of degradation is nonetheless difficult to determine owing to the simultaneous effect of degrading and nondegrading (i.e., dilution, volatilization, sorption) processes on overall contaminant mass dissipation. An additional line of evidence to identify the occurrence of *in-situ* degradation may be obtained with compound-specific isotope analysis (CSIA). CSIA has proven useful to quantify degradation processes of halogenated contaminants under both laboratory (Audí-Miró et al., 2013; Hermon et al., 2018; Renpenning et al., 2014) and field conditions (Blázquez-Pallí et al., 2019; Palau et al., 2016; Wiegert et al., 2012). CSIA relies on changes in stable isotope ratios (e.g., $^{13}C/^{12}C$) produced during a given degradation

reaction in which bond cleavage of molecules containing light isotopes occurs preferentially over those bearing one or more heavy isotopes (Elsner, 2010), resulting in an enrichment of heavy isotopes in the remaining contaminant fraction. When changes of stable isotope ratios of two elements involved in the same bond cleavage reaction (e.g., $^{13}C/^{12}C$ and $^{37}Cl/^{35}Cl$) are compared in a dual plot, the resulting slope (Λ) provides a quantitative parameter of the corresponding contaminant transformation pathway or mechanism (Höhener & Imfeld, 2020; Ojeda et al., 2020).

The relevance of multi-element CSIA (ME-CSIA) was recently demonstrated when investigating the effect of water table fluctuations on dichloromethane (DCM) degradation in laboratory aquifers fed with anoxic contaminated groundwater (Prieto-Espinoza et al., 2021). DCM (CH_2Cl_2) is a toxic industrial halogenated solvent frequently detected in multi-contaminated aquifers, and included in the list of priority pollutants of the U.S. (ASTDR, 2019) and the European Commission (European Commission, 2013). ME-CSIA of DCM (i.e., $^{13}C/^{12}C$ and $^{37}Cl/^{35}Cl$) evidenced larger extent of DCM degradation in laboratory aquifers during water table fluctuations compared to steady-state conditions, and suggested distinct anaerobic DCM degradation pathways. Bacterial populations belonging to the anaerobic *Peptococacceae* family such as *Desulfosporosinus*, *Dehalobacterium* and *Dehalobacter* spp. which include DCM-degrading strains displayed higher relative population size during transient conditions and localized across the fluctuation zone and CF. This suggested oxygen tolerance of these taxa during water table fluctuations and emphasized the role of different bacterial populations during DCM biodegradation (Blázquez-Pallí et al., 2019; Hermon et al., 2018; Wright et al., 2017).

To understand the complex interplay between biogeochemical variations and contaminant degradation in aquifers subjected to water table fluctuations, multi-phase flow reactive transport models (RTMs) may integrate CSIA data and distinct bacterial populations directly or indirectly involved in contaminant degradation. Several RTMs relying on CSIA data

have been successfully applied to evidence contaminant degradation, particularly for chlorinated ethenes (CEs), further demonstrating the promising insights of CSIA in RTMs (Antelmi et al., 2021; Badin et al., 2018; D'Affonseca et al., 2011; Höhener, 2016; Hunkeler et al., 2009; Kuder et al., 2016; Prommer et al., 2009). Nevertheless, such RTMs are often applied in oversimplified configurations (e.g., batch case, steady-state, single bacteria, etc.) compared to field complexity. While advanced numerical approaches have enabled capturing dynamics across the CF (Hron et al., 2015), RTMs accounting for ME-CSIA are still needed to unravel the effect of water table fluctuations on common halogenated solvents at contaminated sites.

Here, we developed and implemented a mathematical formalism describing multi-component and multi-phase flow reactive transport of DCM in aquifers, including the description of six DCM isotopologues (i.e., accounting for $^{13}C/^{12}C$ and $^{37}Cl/^{35}Cl$) and distinct DCM-degrading and nondegrading bacterial populations. The objective of this study was to apply the developed integrative RTM on the experimental setup described in Prieto-Espinoza et al. (2021). Eight model scenarios, including abiotic and biotic conditions, were examined to distinguish the contribution of volatilization and degradation processes on DCM mass dissipation across the aquifer during steady-state (i.e., static water table) and transient (i.e., fluctuating water table) conditions. For all biotic scenarios, DCM degradation was examined using different combinations of bacterial degrading populations, including heterotrophic groundwater bacterial populations, and numerical results were assessed using experimental data.

2. Model formalisms

2.1 Experiment

Experiments were conducted in two laboratory aquifers with inner dimensions of 1.60 m × 0.80 m × 0.05 m (length × height × width) and filled with sterile quartz sand (grain size: 0.4 - 0.6 mm). A detailed description of the experimental setup is provided in Prieto-Espinoza et al. (2021) and as Supporting Information (SI, Section A). Briefly, aquifers were covered by a top glass mounted with 3 sampling ports opened to the atmosphere (Figure 1). Both aquifers were continuously fed with O_2-depleted contaminated groundwater (O_2 < 1 mg/L) and kept under constant N_2-flux. Prior to the experiments, an incubation period was established by operating both aquifers with a continuous flow of DCM-spiked groundwater collected from a former industrial site (Hermon et al., 2018). This allowed to reach initial steady-state conditions. The water table was positioned at a depth of 0.33 m from the bottom of both aquifers. During the experimental phase, one aquifer remained under steady-state conditions while the second aquifer underwent two water table fluctuation events (Figure 1). Hydrochemical species, DCM, stable isotopes and bacteria were followed before and after each water table fluctuation event, and at sampling ports located at 0.15 m and 0.40 m from the bottom. For a detailed description of chemical, isotopes and bacterial analyses we refer to Prieto-Espinoza et al. (2021).

2.2 Main model assumptions

The model formalism includes a state-of-the-art description of three DCM-degrading bacterial populations with partly known DCM degradation pathways (Chen et al., 2018, 2020; Holland et al., 2019; Kleindienst et al., 2017, 2019; Mägli et al., 1996, 1998) and associated stable carbon and chlorine isotope fractionation (Chen et al., 2018; Lee et al., 2015) (Table 1). The model only considers anaerobic DCM-degrading bacteria (*Peptococacceae* family) as O_2-depleted conditions prevailed in the laboratory aquifers (Prieto-Espinoza et al., 2021). Abiotic DCM degradation is not considered in the model due to substantial evidence of biodegradation

as the main DCM dissipation process in contaminated aquifers (Blázquez-Pallí et al., 2019; Hermon et al., 2018; Wright et al., 2017). A non-DCM degrading bacterial population which mineralizes dissolved organic carbon (DOC) and produces CO_2 was additionally included, as CO_2 production by heterotrophic groundwater microorganisms may impact DCM degradation (Chen et al., 2020). Hereafter, this generic population will be named 'heterotrophic' population as it may use many different organic compounds (DOC) as carbon sources.

Simulations were carried out for both steady-state and transient conditions. Mass exchange of six DCM isotopologues was implemented assuming the same rate of gas-phase partitioning and volatilization. A first-order kinetic exchange was also assumed between the gas and water phases for O_2 and CO_2 (Hron et al., 2015). Isotope fractionation of DCM caused by diffusion was not accounted for in the model as it is typically negligible compared to degradation processes (Bouchard et al., 2008; Jeannottat and Hunkeler, 2013). Similarly, DCM sorption and its associated isotope fractionation was not accounted for in the model due to its low log K_{ow} (<1.25) (Merlin et al., 1992). Consumption of all dissolved chemical species was assumed to occur in the water phase only and following a dual-Monod approach. Transformation products of each pathway-specific reaction were also followed, including Cl^-, acetate and formate (Chen et al., 2020). Finally, interactions of dissolved chemical species including electron acceptors (EA) and transformation products (TP) with the solid phase were neglected.

2.3 Multi-phase flow and transport

The model considers two phases (α): a gaseous phase g and an aqueous phase w (for water). The two phases are considered incompressible. Each of these phases have their own volumetric mass density ρ_α [kg/m^3] and saturation s_α. The saturations must satisfy the closure relation $\sum_\alpha s_\alpha = 1$. The mass conservation equation for the flow of each α phase is:

$$\partial_t(\phi s_\alpha) + \nabla \cdot (\boldsymbol{v}_\alpha) = \boldsymbol{Q}_\alpha \quad (1)$$

where $\boldsymbol{v}_\alpha$ is the mean pore velocity [m/s] expressed by the Darcy Muskat's law following $\boldsymbol{q}_\alpha = \phi s_\alpha \boldsymbol{v}_\alpha$, ϕ is the porosity [-], and $\boldsymbol{Q}_\alpha$ is a source term [m^3/s].

For each component *i* present in α phase, the advection-dispersion equations describing reactive transport and mass transfer exchange are written as:

$$\partial_t\left(\epsilon_\alpha c_{\alpha,i}\right) + \nabla \cdot \left(\epsilon_\alpha c_{\alpha,i}\boldsymbol{v}_\alpha + \epsilon_\alpha \boldsymbol{j}_{\alpha,i}\right) = -\epsilon_\alpha r_{\alpha,i} + \sum_{\beta \neq \alpha} e_{\alpha,i}^{\alpha\beta} \quad (2)$$

where $c_{\alpha,i}$ is the mass concentration of component *i* in the α phase [kg/m^3], $\boldsymbol{j}_{\alpha,i}$ is the intrinsic mass dispersion vector [kg/m^2/s], $r_{\alpha,i}$ is the reactive rate [kg/m^3/s] and $e_{\alpha,i}^{\alpha\beta}$ is the rate of mass transfer of component *i* into the α phase at the $\alpha\beta$ interface (dissolution) [kg/m^3/s]. The volume fraction occupied by the α phase is defined as $\epsilon_\alpha = \phi s_\alpha$.

The Fick's law was used to describe diffusion and dispersion fluxes $\boldsymbol{j}_{\alpha,i}$ together with the second model of Millington and Quirk for the dependence of the effective diffusion coefficient on phase saturation (Millington & Quirk, 1961). For mechanical interactions of the fluid with the porous media causing mixing of solutes across the two phases, a diffusion/dispersion tensor was used to estimate the corresponding fluxes:

$$\boldsymbol{j}_{\alpha,i} = -\left(s_\alpha^{10/3}\phi^{4/3} D_{\alpha,i}^{mol}\mathbf{I} + \alpha_t|\boldsymbol{q}_\alpha|\mathbf{I} + (\alpha_l - \alpha_t)\frac{\boldsymbol{q}_\alpha \boldsymbol{q}_\alpha}{|\boldsymbol{q}_\alpha|}\right)\nabla c_{\alpha,i} \quad (3)$$

where α_l and α_t are the longitudinal and transverse dispersivities [m], respectively, and $D_{\alpha,i}^{mol}$ is the molecular diffusion of component *i* in α phase [m^2/s].

Due to capillary effects, average pressure fields of each phase are not equal. A macroscale capillary pressure p_c, depending on the water saturation s_w, was thus defined as $p_c = p_n - p_w$, where p_n is the pressure of the non-wetting phase and p_w the pressure of the wetting phase [Pa]. The p_c values were obtained following the Brooks-Corey model (Brooks & Corey,

1965). A description of mass-momentum conservation equations for the CF is provided as SI (Section B).

2.4 Mass exchange across the capillary fringe

The porous media is considered partially saturated with water and gas phases with a mixture of DCM, O_2 and CO_2. In the case of local non-equilibrium, volatilization of component *i* from the aqueous (*w)* to the gaseous (*g)* phase (and conversely the leaching of component *i* present in the gas phase by re-solubilization), corresponding to the adimensional Henry's constant, is given by (Hron et al., 2015):

$$e_{g,i}^{wg} = \epsilon_g \Gamma_{volat,i} \left(p_i^{sat} \frac{M_{mol,i}}{c_i^{eq} RT} \rho_w \omega_{w,i} - \rho_g \omega_{g,i} \right) = -e_{w,i}^{wg} \quad (4)$$

where $\Gamma_{volat,i}$ is the mass transfer coefficient by volatilization [1/s], c_i^{eq} is the water solubility [kg/m^3], $M_{mol,i}$ is the molar mass [kg/mol] and p_i^{sat} is the saturated vapor pressure of component *i* (pure form) [Pa]. Phase composition (i.e., mass concentration) is relative to the mass fraction of component *i* in α phase (i.e., $\omega_{\alpha,i}$) and the mass phase density (i.e., ρ_w and ρ_g).

2.5 Pathway-specific reaction rates and dual isotope fractionation

Evolution of carbon and chlorine stable isotopes of DCM during biodegradation reactions was simulated accounting for dual-element isotopologues. The relative abundance of the six DCM isotopologues, considering the occurrence of both stable C and Cl isotopes, can be calculated with a binomial distribution (Jin et al., 2018):

$$A_j = \binom{1}{a} X^a (1-X)^{1-a} \binom{2}{b} Y^b (1-Y)^{2-b} \quad (5)$$

where A_j is the relative abundance of the jth DCM isotopologues containing *a* ^{13}C out of a total of one carbon atom and *b* ^{37}Cl out of a total of two chlorine atoms. *X* and *Y* are the relative abundances of heavy C and Cl isotopes, respectively. Double layer brackets represent classical binomial coefficients. The initial C-Cl DCM isotopologues abundance was computed according

to initial isotopic signatures of DCM of $\delta^{13}C_0 = -46.38 \pm 0.37‰$ and $\delta^{37}Cl_0 = 3.68 \pm 0.10‰$, and the international standards of C (VPDB, $R^0_{VPDB} = 0.0112372$) and Cl (SMOC, $R^0_{SMOC} = 0.319766$) isotope ratios (Coplen, 2011; Kaufmann et al., 1984):

$$R^h_{E_0} = \left(\frac{\delta^h E_0}{1000} + 1\right) R^0_{E,std} \quad (6)$$

$$A^h_{E_0} = \frac{R^h_{E_0}}{1+R^h_{E_0}} \quad (7)$$

where $R^h_{E_0}$ is the initial DCM isotope ratio, $\delta^h E_0$ is the initial DCM isotopic signature, and $R^0_{E,std}$ is the international standard of element *E*. $A^h_{E_0}$ is the relative abundance of stable heavy isotopes of element *E*, so that the abundance of light isotopes of *E* is given by $A^l_{E_0} = 1 - A^h_{E_0}$. Note that the terms *X* and *Y* in equation 5 correspond to the abundances of heavy C and Cl isotopes, respectively, calculated with equation 7.

During a given reaction of an organic contaminant the stable isotopes present in the bond cleavage are primarily affected (position-specific isotopes). Position-specific isotope fractionation factors for the j^{th} DCM isotopologues are thus calculated to account for the number of atoms at the reactive position (Elsner, 2010):

$$\alpha^\kappa_E = \frac{1}{AKIE^\kappa_E} \approx 1 + \frac{n_E}{z_E}\varepsilon^\kappa_E \quad (8)$$

where α^κ_E is the fractionation factor of element *E* (i.e., C and Cl) at the reactive position. ε^κ_E is here referred to as the *bulk* enrichment factor [in ‰], n_E is the number of atoms of element *E*, and z_E is the number of atoms at the reactive position. In the case of DCM, chemically composed by 1 C atom and 2 Cl atoms, we consider that $n_C = a = 1$ and $n_{Cl} = b = 2$. Reactive positions will thus be affected with $z_C = 1$ and $z_{Cl} = 2$.

Let's κ be the κ-bacterial population involved in the pathway-specific degradation reaction of DCM (section 2.6). The C and Cl isotope fractionation factors for each κ-bacterial

246 population are assigned to pathway-specific degradation reactions (Jin et al., 2018). These
247 fractionation factors affect overall reaction rates of each jth position-specific isotopologue of
248 DCM (see Eq. 17).

249 $$\alpha_j^{\kappa} = \alpha_C^{\kappa,a_j} \alpha_{Cl}^{\kappa,b_j} \quad (9)$$

250 The $\Lambda^{C/Cl}$ values associated with changes of C *versus* Cl isotope signatures provide
251 evidence of the corresponding DCM degradation pathway or mechanism by the κ-bacterial
252 population, and can be calculated as (Höhener & Imfeld, 2021; Ojeda et al., 2020):

253 $$\Lambda^{C/Cl} = \frac{ln[(\delta^{13}C_t/1000+1)/(\delta^{13}C_0/1000+1)]}{ln[(\delta^{37}Cl_t/1000+1)/(\delta^{37}Cl_0/1000+1)]} \approx \frac{\varepsilon_{bulk}^{C}}{\varepsilon_{bulk}^{Cl}} \quad (10)$$

254 Finally, the degradation extent of DCM (*B*, in %) was estimated according to Van
255 Breukelen (2007) using a modified version of the Rayleigh equation in which the rate ratio of
256 two competing degradation pathways can be accounted for.

257 $$B\ (\%) = \left(1 - \left(\frac{\delta^h E_t+1000}{\delta^h E_0+1000}\right)^{\frac{1000}{(F\varepsilon_E^{\kappa,1}+(1-F)\varepsilon_E^{\kappa,2})}}\right) \times 100 \quad (11)$$

258 Here, *F* is the contribution factor of a degradation pathway concomitantly transforming DCM
259 as a function of the apparent $\Lambda^{C/Cl}$ and ε_E^{κ} values of element *E* associated with the two pathways
260 (Van Breukelen, 2007):

261 $$F = \frac{\Lambda^{C/Cl}\varepsilon_{Cl}^{\kappa,2} - \varepsilon_C^{\kappa,2}}{(\varepsilon_C^{\kappa,1} - \varepsilon_C^{\kappa,2}) - \Lambda^{C/Cl}(\varepsilon_{Cl}^{\kappa,1} - \varepsilon_{Cl}^{\kappa,2})} \quad (12)$$

262 **2.6 DCM biodegradation by distinct κ-bacterial populations**

263 Three distinct anaerobic DCM degradation pathways were considered to represent the
264 activity of co-occurring DCM-degraders in polluted aquifers (Table 1) (Blázquez-Pallí et al.,
265 2019; Hermon et al., 2018; Lee et al., 2015; Wright et al., 2017). These correspond to anaerobic
266 DCM degradation by simulated populations of (i) *Dehalobacter*-containing culture under iron-

267 reducing conditions (Lee et al., 2015) Dhber (X_1), (ii) *Dehalobacterium formicoaceticum* (Chen
268 et al., 2020; Kleindienst et al., 2019) Dhbium (X_2), and (iii) *Candidatus* Dichloromethanomonas
269 elyunquensis (Chen et al., 2018, 2020; Kleindienst et al., 2019) Diely (X_3). Mineralization of
270 DOC was also considered and mediated by heterotrophic non-DCM degrading bacteria denoted
271 B_{DOC} (X_4) under both aerobic and iron-reducing conditions. Such microorganisms produce CO_2
272 as final product, which can be further utilized during DCM metabolism by Dhbium and Diely
273 (Chen et al., 2020).

Table 1. κ-bacterial populations involved in anaerobic DCM degradation, and corresponding pathway-specific reactions based on stable carbon and chlorine isotope fractionation values. The results of laboratory aquifers under steady-state and transient conditions are also provided for comparison.

Name	κ-bacterial populations	ε_C (‰) [a]	ε_{Cl} (‰) [a]	$\Lambda^{C/Cl}$ [a]	Degradation pathway	Redox reactions	Source
Simulated anaerobic DCM degrading populations							
X1 (Dhber)	*Dehalobacter* containing culture	−15.5±1.5	−5.3±0.1[b]	2.92 [c]	Fermentation	$CH_2Cl_2 + 2H_2O + Fe^{3+} \rightarrow CO_2 + Fe^{2+} + 6H^+ + 6Cl^-$	Lee et al., 2012, 2015
X2 (Dhbium)	*Dehalobacterium formicoaceticum*	−42.4±0.7	−5.3±0.1	7.89±0.12	Fermentation harboring WLP [d]	$3CH_2Cl_2 + 4H_2O + CO_2 \rightarrow 2HCOO^- + CH_3COO^- + 9H^+ + 6Cl^-$	Chen et al., 2018, 2020
X3 (Diely)	Consortium RM harboring *Ca.* Dichloromethanomonas elyunquensis	−18.3±0.2	−5.2±0.1	3.40±0.03	Mineralization (acetogenesis required) [e]	$CH_2Cl_2 + 2H_2O \rightarrow CO_2 + 2H_2 + 2Cl^- + 2H^+$ $4H_2 + 2CO_2 \rightarrow CH_3COO^- + H^+$	Chen et al., 2018, 2020
Simulated heterotrophic groundwater bacterial population (DOC assimilation)							
X4 (B_{DOC})	Heterotrophic bacteria	-	-	-	Aerobic respiration	$CH_2O + O_2 \rightarrow CO_2 + H_2O$	Rolle et al., 2008
		-	-	-	Iron reduction [f]	$CH_2O + Fe^{3+} + H_2O \rightarrow Fe^{2+}\ CO_2 + 4H^+$	Rolle et al., 2008
Laboratory aquifers							
Transient conditions	*Dehalobacter*, *Dehalobacterium*, *Desulfosporosinus* [g]	−11.8±2.0	−3.1±0.6	3.58±0.42	Prevailing anaerobic	n.a.[h]	Prieto-Espinoza et al., 2021
Steady-state conditions		−23.6±3.2	−8.7±1.6	1.92±0.30	Prevailing anaerobic	n.a.	Prieto-Espinoza et al., 2021

[a] Uncertainties of ε and Λ values correspond to the 95% confidence interval (CI).
[b] Assumed ε^{Cl} (‰) value for a *Dehalobacter* containing culture.
[c] Estimation of $\Lambda^{C/Cl}$ was based on assumed Cl isotope fractionation.
[d] Wood Ljundhal Pathway (Ragsdale et al., 2008).
[e] DCM mineralization by *Ca.* D. elyunquensis requires the presence of H_2-consuming partner populations.
[f] This model assumes the presence of aqueous Fe^{3+} species.
[g] Most abundant taxa observed in the laboratory aquifers.
[h] n.a.: values were not analyzed/derived.

Stoichiometry of redox reactions were used to approximate biomass growth and evolution of redox species (Barry et al., 2002; Rittmann, 2006) based on pathway-specific degradation reactions of DCM (Chen et al., 2018, 2020; Lee et al., 2015). All bacterial populations relied on the availability of dissolved O_2, Fe(III) and/or CO_2 species. Growth equations (Table 2) were estimated assuming that 50% of the carbon sources (i.e., DCM and CO_2) were required for the synthesis of new biomass ($C_5H_7O_2N$) (Eckert et al., 2012). A detailed description of growth stoichiometry reactions is given in the SI (Section C).

Table 2. Estimated growth reactions of κ-bacterial populations for DCM and DOC degradation.

Name	Growth reactions
X_1 (Dhber)	$CH_2Cl_2 + 2Fe^{3+} + 1.2H_2O + 0.1NH_4^+ \rightarrow 0.5CO_2 + 0.1C_5H_7O_2N + 2Fe^{2+} + 4.1H^+ + 2Cl^-$
X_2 (Dhbium)	$CH_2Cl_2 + 0.9H_2O + 0.15CO_2 + 0.1NH_4^+ \rightarrow 0.1C_5H_7O_2N + 0.35HCOO^- + 0.15CH_3COO^- + 2.7H^+ + 2Cl^-$
X_3 (Diely)	$CH_2Cl_2 + 0.88H_2O + 0.1NH_4^+ \rightarrow 0.1C_5H_7O_2N + 0.17CO_2 + 0.17CH_3COO^- + 0.33H_2 + 2.29H^+ + 2Cl^-$
X_4 (B_{DOC},,ox)	$CH_2O + 0.5O_2 + 0.1NH_4^+ \rightarrow 0.5CO_2 + 0.1C_5H_7O_2N + 0.1H^+ + 0.8H_2O$
X_4 (B_{DOC},anox)	$CH_2O + 2Fe^{3+} + 0.2H_2O + 0.1NH_4^+ \rightarrow 0.5CO_2 + 0.1C_5H_7O_2N + 2Fe^{2+} + 2H^+$

2.7. Modeling of bacterial dynamics

Active bacterial growth was set in both the aqueous and on the solid (*s*) phases, and depended on the presence of carbon substrates (i.e., DCM and DOC) and electron acceptors (i.e., O_2, Fe(III), CO_2). Total bacterial concentration (c_{X_κ}) in the aquifer was thus defined as:

$$c_{X_\kappa} = c_{w,X_\kappa} + c_{s,X_\kappa}\frac{\epsilon_s}{\epsilon_w} \quad (13)$$

where c_{w,X_κ} and c_{s,X_κ} are the bacterial concentrations in the aqueous phase (i.e., planktonic) [kg/m^3] and on the solid phase (i.e., attached) [kg/m^3], respectively. Planktonic biomass in the aqueous phase was considered using the classical advection-dispersion formulation (Eq. 2). The biomass bound to the solid matrix was assumed immobile and its volume sufficiently low to avoid changes in the permeability and clogging. The solid phase mass balance equation for κ-bacterial solid concentrations c_{s,X_κ} is given by Eq. 14. Evolution of biomass on the solid phase

299 is affected by bacterial attachment-detachment processes (Section 2.7.1) and growth kinetics
300 (Section 2.7.2; Eq. 25).

301 $$\frac{\partial \epsilon_s c_{s,X_\kappa}}{\partial t} = -r_{s,X_\kappa} \quad (14)$$

302 **2.7.1 Bacterial attachment-detachment in porous media**

303 In order to evaluate κ-bacterial transport and attachment in the saturated and unsaturated
304 porous media, bacterial adhesion to sand grains was included following a reversible formulation
305 involving an adhesion term a_{w,X_κ} from the aqueous phase (Hron et al., 2015):

306 $$a_{w,X_\kappa} = -\epsilon_w k_\kappa^{att} \psi_\kappa c_{w,X_\kappa} + \epsilon_s k_\kappa^{det} c_{s,X_\kappa} \quad (15)$$

307 where k_κ^{att} and k_κ^{det} are the first order deposition and detachment coefficients for the κ-bacterial
308 population [1/s], respectively. ψ_κ is a dimensionless [-] deposition function that relates adhesion
309 to solid surface with water saturation (Hron et al., 2015):

310 $$\psi_\kappa = 1 - \frac{c_{s,X_\kappa}}{s_w c_{s,X_\kappa}^{max}} \quad (16)$$

311 where c_{s,X_κ}^{max} is the κ-specific maximum attainable bacterial concentration on the solid phase
312 [kg/m^3].

313 **2.7.2 Bacterial growth kinetics**

314 Growth kinetics of κ-bacterial populations are limited by the availability of dissolved
315 oxygen (c_{w,O_2}), ferric iron ($c_{w,Fe}$), carbon dioxide (c_{w,CO_2}), DOC ($c_{w,DOC}$) and bioconvertible
316 jth isotopologues of DCM ($c_{w,j}$). Both planktonic and attached bacteria are able to consume
317 substrates. New biomass is considered immediately mobile in the aqueous phase and can attach
318 onto solid grains. Specific bacterial growth rates were based on the Contois model (Contois,
319 1959). The Contois modification describes variations of half-saturation constants in Monod
320 models during one growth cycle (i.e., the dependence of μ_{max} on the biomass density)

(Kovárová-Kovar & Egli, 1998). Pathway-specific reaction rates based on C and Cl isotopes were also introduced for κ-bacterial populations involved in DCM degradation (κ = 1, 2, 3) (see Section 2.5).

$$r_j^{\kappa} = \mu_{max}^{k} \frac{\alpha_C^{\kappa,a_j} \alpha_{Cl}^{\kappa,b_j} c_{w,j}}{c_{X_\kappa} B_{DCM}^{\kappa} + c_{w,DCM}} \frac{c_{w,EA_\kappa}}{c_{X_\kappa} B_{EA}^{\kappa} + c_{w,EA_\kappa}} \quad (17)$$

where μ_{max}^{κ} is the specific growth rate [1/s] of the κ-specific degradation pathway involving iron-reduction, fermentation or anaerobic mineralization of DCM (Table 3). $c_{w,DCM}$ is the total DCM concentration, such as $c_{w,DCM} = \sum_j^N c_{w,j}$, where j=1,$\mathcal{N}$ with $\mathcal{N}$=6 is the total number of DCM isotopologues. The constant B [-] multiplied by c_{X_κ}, introduced as the Contois modification, corresponds to the half-saturation constant in Monod kinetics. Electron acceptors (EA) for each degradation pathway are introduced with a dual Monod term. Oxygen inhibition terms were not accounted for in the model due to high abundance (up to 80%) of putative anaerobic bacterial populations in the fluctuation zone and CF of the laboratory aquifers (Prieto-Espinoza et al., 2021). This high bacterial abundance coincided with DCM metabolic activity, indicative of tolerance to temporal O_2 variations associated with water table fluctuations.

For DOC assimilation, it was assumed that bacterial growth occurs in the presence of both O_2 and ferric iron (Hron et al., 2015).

$$r_{w,DOC}^{ox} = \mu_{max}^{ox} \frac{c_{w,DOC}}{c_{X_4} B_{DOC}^{4} + c_{w,DOC}} \frac{c_{w,O_2}}{c_{X_4} B_{O_2}^{4} + c_{w,O_2}} \quad (18)$$

$$r_{w,DOC}^{anox} = \mu_{max}^{anox} \frac{c_{w,DOC}}{c_{X_4} B_{DOC}^{4} + c_{w,DOC}} \frac{c_{w,Fe}}{c_{X_4} B_{Fe}^{4} + c_{w,Fe}} \quad (19)$$

The global reactive terms for the jth isotopologues of DCM and DOC and the consumption of EA during degradation of both carbon sources by the corresponding κ-bacterial population have the following form:

$$r_{w,j} = \sum_{\kappa=1}^{3} \frac{r_j^{\kappa}}{Y_{X_{\kappa/j}}} c_{X_\kappa} \quad (20)$$

$$r_{w,DOC} = \left(\frac{r_{w,DOC}^{ox}}{Y_{X_{4/DOC}}^{ox}} + \frac{r_{w,DOC}^{anox}}{Y_{X_{4/DOC}}^{anox}} \right) c_{X_4} \quad (21)$$

$$r_{w,EA} = \sum_{\kappa=1}^{3} E_{\mathrm{EA/j}}^{\kappa} \frac{r_j^{\kappa}}{Y_{X_{\kappa/j}}} c_{X_\kappa} + \left(E_{\mathrm{EA/DOC}}^{4,ox} \frac{r_{w,DOC}^{ox}}{Y_{X_{4/DOC}}^{ox}} + E_{\mathrm{EA/DOC}}^{4,anox} \frac{r_{w,DOC}^{anox}}{Y_{X_{4/DOC}}^{anox}} \right) c_{X_4} \quad (22)$$

For each transformation product (i.e., Cl^-, acetate, formate and CO_2), the corresponding reactive term has the form:

$$r_{w,TP} = -\sum_{j}^{\mathcal{N}} \sum_{\kappa} \Upsilon_{TP,j}^{\kappa} \frac{r_j^{\kappa}}{Y_{X_{\kappa/j}}} c_{X_\kappa} - \left(\Upsilon_{\mathrm{TP/DOC}}^{4,ox} \frac{r_{w,DOC}^{ox}}{Y_{X_{4/DOC}}^{ox}} + \Upsilon_{\mathrm{TP/DOC}}^{4,anox} \frac{r_{w,DOC}^{anox}}{Y_{X_{4/DOC}}^{anox}} \right) c_{X_4} \quad (23)$$

where yield factor coefficients $Y_{X_{\kappa/j}}$ [biomass X_κ produced in g per mass of organic substrate *j* biodegraded in g], $E_{\mathrm{EA/j}}^{\kappa}$ [g of electron acceptor (*EA*) consumed per mass of organic substrate *j* biodegraded in g] and $\Upsilon_{TP/j}$ [g of transformation product (TP) produced per mass of organic substrate *j* biodegraded in g] are associated with pathway-specific reaction rates (Table 3). The second terms of Eq. 22 and Eq. 23 are only valid for species affected by B_{DOC} (X_4; Table 3).

The multi-phase flow reactive transport equations of DCM biodegradation by three distinct DCM-degrading populations and in the presence of heterotrophic groundwater bacterial populations are presented in the SI (Section D). The reactive terms of the κ-bacterial populations, denoting biomass growth and decay (k_κ^{dec}; constant rate) in the aqueous and on the solid phases, are given by:

$$r_{w,X_\kappa} = -\epsilon_w \sum_{j}^{\mathcal{N}} r_j^{\kappa} \left(1 - \frac{c_{X_\kappa}}{c_{X_\kappa}^{max}} \right) - a_{w,X_\kappa} \quad (24)$$

$$r_{s,X_\kappa} = \epsilon_s k_\kappa^{dec} c_{s,X_\kappa} + a_{w,X_\kappa} \quad (25)$$

3. Modeling approach

3.1 Numerical resolution

A detailed description of the numerical resolution is described in the SI (Section E). The flow is solved by an IMPES scheme (IMplicit in gas Pressure and Euler Explicit in water Saturation) with a finite volume discretization centered on the nodes (CVFE). The linear solver for the gas phase is a preconditioned conjugate gradient (PCG). A Courant criterion is imposed for saturation (0.5) allowing higher time steps (~ 2.7 sec) for explicit resolution of water saturation and to take capillary diffusion and gravity effects into account. Following the Method Of Line (MOL) framework, the transport (non-symmetric matrix) is solved with a large-scale preconditioned differential-algebraic solver using a Krylov method (DASPK) (Brown et al., 1994) and by performing an adaptive time-step strategy based on interpolation of previous time solutions (Backward Differentiation Formula 'BDF' scheme). A linear solver for the non-symmetric matrix is used following a preconditioned biconjugate gradient method (PBiCGStab). A variant called cubicmIsotopFoam integrating a distributed parallelization is implemented (PStream library of OpenFoam 9 solver; Weller et al., 1998) to handle massively parallel cases. The numerical code is integrated in a user interface coded in python (3.10.2) and based on the Qt 15.2 library (Qt group, 2023) initially coded with DISLIN (Michels, 1998).

3.2 Model domain and boundary conditions

Model simulations were carried out in 2D on a tank with the same dimensions as the laboratory aquifers (Figure 1 and Section 2.1). Hydrodynamic parameters (porosity, capillary parameters, K_{sat}) were determined using k_r-p_c curves (data not shown). The modeled tank had 1808 elements of size 5 × 5 cm. Coordinates along x-axis of the headspace ports were 0.20 m, 0.80 m and 1.4 m, with 0.05 m width. Atmospheric pressure and equilibrium gas concentrations of O_2 and CO_2 were imposed at the top of the domain.

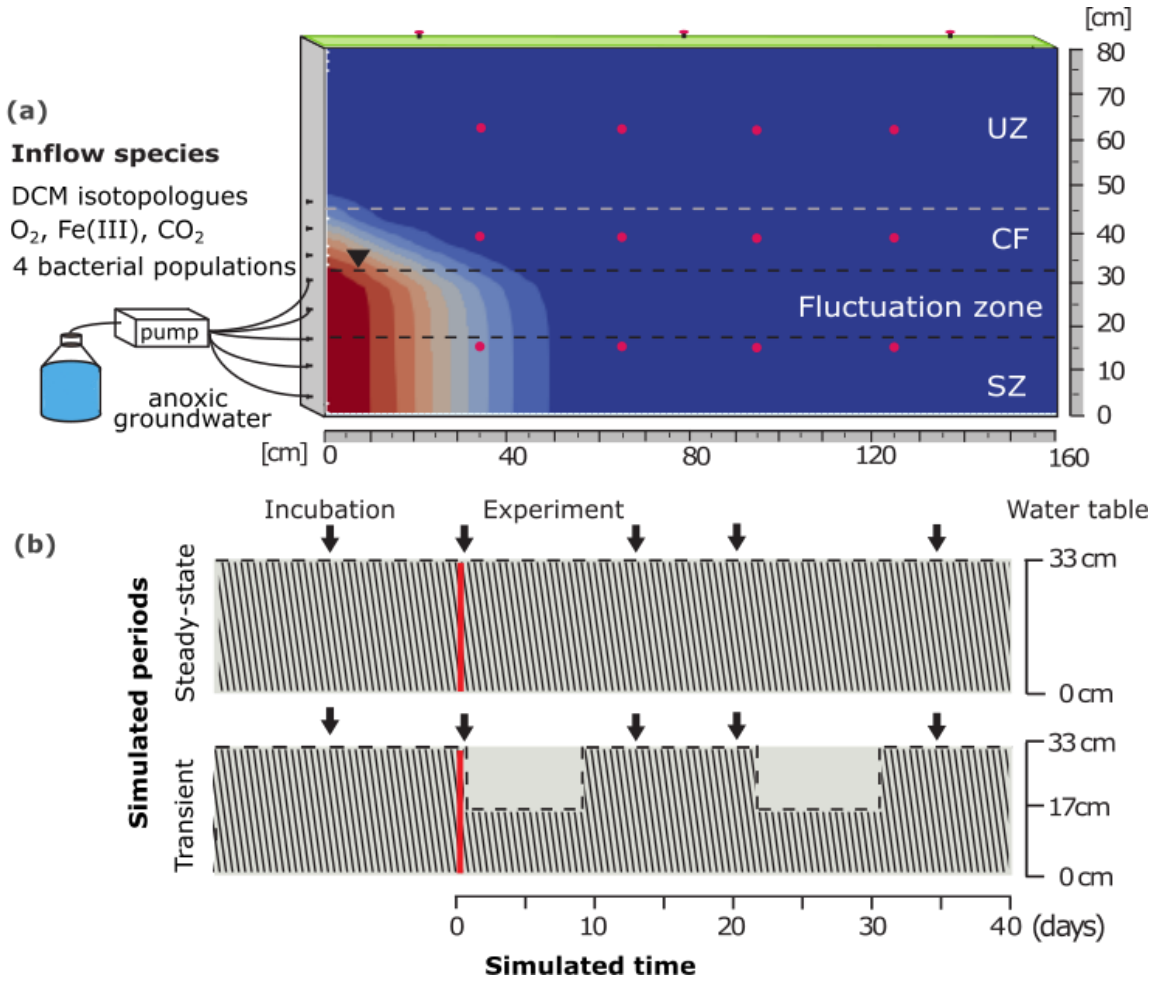

Figure 1. Simulated model domain based on the laboratory aquifers setup. (a) Schematic overview of the aquifers fed with anoxic groundwater spiked with DCM (flow path from left to right), indicating the saturated zone (SZ), unsaturated zone (UZ), fluctuation zone, position of sampling ports (red dots), and top boundary layer (green) with three sampling ports opened to the atmosphere. (b) Simulated steady-state and transient periods. Water table level is indicated as dotted lines. The end of the incubation period (total 60 days) is marked with a red line. Simulations of the two flow regimes (experimental phase) are performed for the period between 0 and 40 days. Black arrows show sampling events of water and gas samples in the experiments at 0, 13, 20 and 35 days.

Initial conditions were set by simulating a free drainage starting from a situation where the porous medium was saturated with anoxic water free of DCM (isotopologues) and O_2. Dissolved biomass, ferric iron and DOC were initially present only during biotic simulations to initiate DCM biodegradation across the CF. Initial concentrations of all species corresponded to those imposed at the inflow of the laboratory aquifers. The biomass attached onto the solid

400 phase was initially set to zero. The saturation level at the top of the domain was maintained at
401 a residual saturation s_{wr} of 8.7%. The fluctuation zone was set in the geometry with boundaries
402 positioned at 0.17 m from the bottom, corresponding to the lower water level kept in the
403 experiments (Figure 1). All domain boundaries, excluding inlet and outlet sides, were
404 impermeable for the aqueous phase (i.e., zero Neumann boundary condition). For the gas phase,
405 all but the top sides were impermeable.

406 Parameters for all simulations and inflow concentrations followed the experimental
407 setup (Table 3 and SI, Section F). A total of 100 days were simulated including an incubation
408 phase of 60 days followed by an experimental phase of 40 days (Figure 1). The simulated time
409 is described from day 0 (i.e., end of the 60-day incubation period) until 40 days (i.e., end of the
410 experiment) (Figure 1b). Continuous injection of DCM (40 mg/L), DOC (100 mg/L), ferric iron
411 (3 mg/L), O_2 (0.25 mg/L) and biomass X_κ (0.01 mg/L) were set at the inflow of the aquifer.
412 After the incubation period, simulations of steady-state consisted on a continuous DCM
413 injection for 40 days (Figure 1b). For transient conditions, the first lowering of the water table
414 took place at day 0 (i.e., end of incubation period) for 1 day, followed by injection of DCM and
415 dissolved species for 7 days at a now low water table (z = 0.17 m). The water table was then
416 raised to its original position (z = 0.33 m) for 1 day and injection of dissolved species was kept
417 until day 21 (Figure 1b). A similar second water table fluctuation occurred from days 21 to 30
418 and continuous injections followed until the end of the experiment.

Table 3. Kinetic parameters of pathway-specific reactions of DCM degradation according to j[th] isotopologues of DCM and electron acceptors (EA) and during concomitant DOC assimilation. When a κ-bacterial population is absent its corresponding aqueous concentration was set to zero.

Kinetic parameters	**κ-bacterial populations DCM degradation**			**Facultative heterotroph for DOC assimilation**	
	Dhber (X_1)/Fe^{3+}	Dhbium (X_2)/CO_2	Diely (X_3)/CO_2	B_{DOC} ($X_{4,ox}$)/O_2	B_{DOC} ($X_{4,anox}$)/Fe^{3+}
μ_{max}^{κ} [1/s]	2.0×10^{-6}	1.0×10^{-6}	1.0×10^{-6}	1.0×10^{-5}	1.0×10^{-7}
k_{κ}^{dec} [1/s]	2.3×10^{-9}	2.3×10^{-9}	2.3×10^{-9}	2.3×10^{-9}	2.3×10^{-9}
k_{κ}^{att} [1/s]	3.0×10^{-4}	3.0×10^{-4}	3.0×10^{-4}	3.0×10^{-4}	3.0×10^{-4}
k_{κ}^{det} [1/s]	6.2×10^{-6}	6.2×10^{-6}	6.2×10^{-6}	6.2×10^{-6}	6.2×10^{-6}
$E_{EA/i}$ [g of EA consumed/g of C source degraded]	1.315	0.078	0.088	0.533	3.723
$Y_{X_{\kappa/i}}$ [g of biomass/g of C source degraded]	0.133	0.133	0.133	0.027	0.027
$Y_{CO_{2/i}}$ [g of CO_2 produced/g of C source degraded]	0.965	-	-	0.733	0.733
$Y_{Cl,j}$ [g of Cl^- produced/g of j[th] DCM degraded]	0.835	0.835	0.835	-	-
Y_{HCOO^-} [g of $HCOO^-$ produced/g of j[th] DCM degraded]	-	0.243	0.118	-	-
Y_{CH3COO^-} [g of CH_3COO^- produced/g of j[th] DCM degraded]	-	0.080	-	-	-
B_i^{κ} [-]	3	3	3	-	-
B_{DOC}^{4} [-]	-	-	-	1.8	1.8
B_{EA}^{κ}	0.019	0.019	0.019	0.019	0.019

3.3 Modeled scenarios

Multi-phase flow and transport – without reactions – was first tested under steady-state (model A) and transient (model B) conditions to examine the ability of the model to reproduce spatial and temporal dynamics of DCM and O_2. These simulations allowed to quantify the extent of DCM volatilization from the saturated zone (SZ) to the unsaturated zone (UZ) under both flow regimes. For simulations where reactions were present, anaerobic DCM degradation was tested by one or several of the κ-bacterial degrading populations in the presence of the non-DCM degrader B_{DOC} (Table 1). These simulations allowed to examine (i) redox dynamics driven by individual κ-bacterial degrading populations under steady-state conditions (models C, D and E), (ii) concomitant DCM degradation under steady-state conditions (models F and G), and (iii) concomitant DCM degradation under transient conditions (models H and I). The main kinetic parameters and modeled scenarios are provided in Tables 3 and 4, respectively. Numerical simulations are successively presented in the results section from scenarios A to I.

Table 4. Description of the eight modeled scenarios. Models A and B were compared with O_2 data from the laboratory aquifers, while models G and I were compared with experimental data of DCM concentrations and stable C and Cl isotopes of DCM.

Transport scenarios			
Scenario	**Conditions**	**κ-bacterial population**	**Purpose**
Model A	Steady	abiotic transport	Multi-phase flow of O_2 and CO_2 across the capillary fringe and DCM volatilization
Model B	Transient	abiotic transport	
Reactive transport scenarios			
Scenario	**Conditions**	**κ-bacterial population**	**Purpose**
Model C	Steady	Dhber and B_{DOC}	Linking redox conditions, heterotrophic groundwater bacteria and DCM biodegradation by κ-bacterial populations under steady-state
Model D	Steady	Dhbium and B_{DOC}	
Model E	Steady	Diely and B_{DOC}	
Model F	Steady	Dhbium, Diely and B_{DOC}	Insights from multiple κ-bacterial populations and heterotrophic groundwater bacteria during DCM biodegradation under static *vs.* water table fluctuations
Model G	Steady	Dhber, Dhbium, Diely and B_{DOC}	
Model H	Transient	Dhbium, Diely and B_{DOC}	
Model I	Transient	Dhber, Dhbium, Diely and B_{DOC}	

3.4 Evaluation strategy and model validation

The numerical methods implemented in this work allow to obtain mechanistic details on multi-phase flow and reactive transport processes affecting DCM dissipation in the laboratory aquifers and particularly across the CF and the fluctuation zone. In total, the 2D-model included 29 non-linear coupled equations with 74 parameters, accounting for the evolution of α phase saturation, capillary pressure, 8 reactive species in both aqueous and gas phases (i.e., the six DCM isotopologues, O_2 and CO_2), 9 species in the aqueous phase (i.e., Fe(III), DOC, Cl^-, acetate, formate, and 4 planktonic bacterial populations), and 4 bacterial populations on the solid phase (attached biomass).

The calibration of this model based on experimental results presented in Prieto-Espinoza et al., (2021) was beyond the scope of this work. This would require long-term investment owing to the large number of parameters, sensitivity of model outputs, and constraints of CPU time (Execution time: 7186 s). Nevertheless, comparisons between numerical model outputs and laboratory experiments without model calibration relating to multi-phase flow across the CF are suitable for a first optimization (Hron et al., 2015), which is the scope of the present study. The model was thus validated based on its ability to capture the trends of key variables

observed in previous laboratory experiments. This may help to understand the processes affecting DCM biodegradation during water table fluctuations.

4. Results

4.1 Multi-phase flow across the capillary fringe

Mass exchange across the CF was examined for O_2, CO_2 and DCM for the non-reactive transport cases under both steady-state (model A) and transient (model B) conditions. The water-retention curve of the aquifer model was well described according to the Brooks and Corey parametrization (Brooks and Corey, 1965), resulting in a sharp increase of the water content across the CF (black line; Figure 2a). The numerical model captured aqueous O_2 profiles formed during O_2 diffusion from the top of the aquifer toward the steady anoxic SZ (Figure 2a). Limited O_2 transfer was observed at high water saturation levels. Contrastingly, water table fluctuations resulted in a re-oxygenation of the underlying groundwater after drainage, establishing saturated O_2 concentrations across the fluctuation zone (z = 0.17-0.33 m; Figure 2b) from 0 to 6 days. Conversely, the inflow of anoxic groundwater then allowed to re-establish both the water table to its original position and the anoxic conditions in the SZ (day 8 onwards; Figure 2b). On the other hand, vertical CO_2 profiles were similar to that of O_2 under steady-state conditions (Figure 2c). During transient conditions, downward diffusion of CO_2 was observed after drainage. However, dissolved CO_2 concentrations in the SZ remained up to 0.5 mg/L (Figure 2d) when the water table reached its initial position, likely due to its higher solubility than that of O_2.

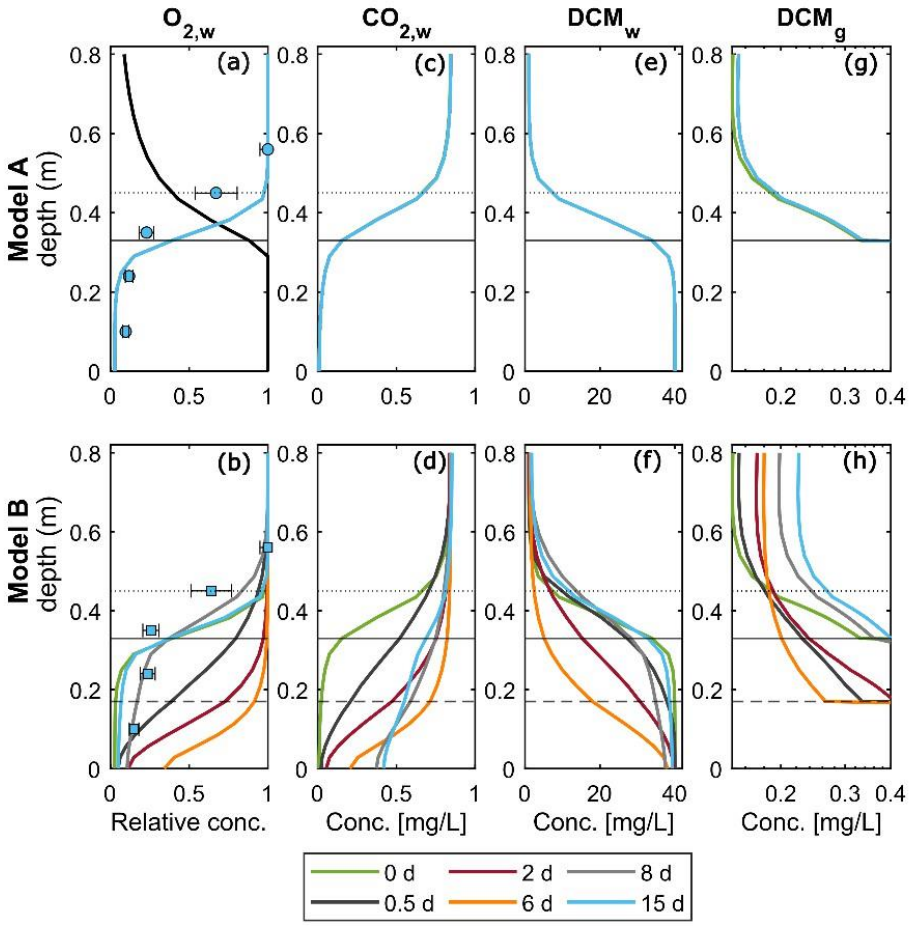

477

478 Figure 2. Depth profiles of (a, b) O_2, (c, d) CO_2, (e, f) DCM aqueous concentrations, and (g, h)
479 DCM gas-phase concentrations in simulated laboratory aquifers under steady-state (top; model
480 A) and transient (bottom; model B) conditions. Depth profiles were retrieved at x = 0.65 m and
481 correspond to one water table fluctuation event (0-15 d). (a) Black line represents the water
482 saturation profile at 15 d, and (a, b) symbols represent data measurements of O_2 aqueous
483 concentrations under steady-state (circles) and transient (squares) conditions at 15 d. Horizontal
484 lines represent the initial position of the water table (z = 0.33 m). Dashed horizontal lines
485 represent the position of the low water table during fluctuation events (z = 0.17 m). Dotted lines
486 represent the upper layer of the CF (z = 0.45 m).

487

488 Under steady-state conditions, steep DCM aqueous concentration gradients were also
489 established across the CF after continuous horizontal flow of DCM for 60 days. The upper layer
490 of the CF (z = 0.45 m) featured a drop in DCM concentrations by approximately 90% compared
491 to the SZ (Figure 2e). DCM gas concentrations remained low (< 50 µg/L) and constant across
492 the upper UZ (Figure 2g). On the other hand, simulated transient conditions showed that as
493 DCM aqueous concentrations dropped across the fluctuation zone after drainage (z = 0.17-0.33

cm), an increase in DCM gas concentrations occurred above the CF (< 300 µg/L; Figure 2h). However, they rapidly decreased when the water table was raised (Figure 2f), indicating that diffusive volatilization was temporarily present during transient conditions and restricted by the slow horizontal groundwater flow.

Monitoring of DCM aqueous concentrations and stable isotopes during abiotic and biotic scenarios (models C-I) allowed to distinguish the contribution of DCM volatilization and biodegradation processes. Overall, volatilization accounted for 10% of DCM mass dissipation during steady-state conditions (models C-G) and approximately 16% during water table fluctuations (models H-I; Table 5). These results are consistent with estimations of volatilization in the laboratory aquifers coinciding with undetected gaseous DCM across the UZ (Prieto-Espinoza et al., 2021).

4.2 DCM biodegradation by individual DCM-degraders in the presence of a heterotrophic bacterial population under steady-state conditions

DCM biodegradation by individual κ-bacterial populations was examined under steady-state flow conditions along with the evolution of redox conditions. During the simulated incubation period (i.e., 60 days of continuous DCM injection to initiate the experimental and model domain), DCM mass dissipation in the SZ accounted for up to 12% of DCM mass removal for Dhber (model C), 17% for Dhbium (model D) and 17% for Diely (model E). Here, planktonic biomass of Dhber increased by 13%, while both Dhbium and Diely increased by 25% (x = 1.60 m). These numerical results thus support the notion that an incubation period prior to the experiments allows for the development of an acclimated degrading bacterial community in the laboratory aquifers (Prieto-Espinoza et al., 2021, 2023). During the experimental phase, numerical results showed a gradual increase of DCM mass dissipation to up to 27% at day 35 for both Dhbium (X_2) and Diely (X_3). However, DCM mass dissipation by Dhber (X_1) remained low <12% (Table 5). This indicated that slow degradation of DCM

occurred via the X_1-pathway which was restricted by low Fe(III) availability (inflow: 3 mg/L) and competition with the heterotrophic bacterial population B_{DOC} for this EA during DOC assimilation.

Table 5. Experimental results and simulated DCM degradation extent (%) and corresponding C and Cl isotopes fractionation for the different model scenarios at day 35 (experimental phase), including the contribution of the incubation phase. Degradation pathways and modeled scenarios are provided in Tables 1 and 4, respectively.

	DCM mass dissipation (%)[a]	Extent of DCM degradation (%)[b]	$\Delta\delta^{13}C$ (‰)[c]	$\Delta\delta^{37}Cl$ (‰)[c]	ε_C (‰)[d]	ε_{Cl} (‰)[d]	$\Lambda^{C/Cl}$ [e]
Modeled scenarios							
Model C	12	2	0.3	0.1	–15.1	–5.1	2.98
Model D	25	18	7.3	1.0	–41.5	–5.2	8.00
Model E	27	18	3.4	1.0	–17.8	–5.1	3.51
Model F	41	35	11.5	2.1	–24.9	–4.4	5.59
Model G	43	36	11.9	2.2	–25.1	–4.4	5.62
Model H	92	76	37.4	6.7	–10.9	–1.9	5.76
Model I	95	79	39.4	6.2	–11.3	–2.0	5.70
Laboratory aquifers (experiments)							
Steady-state	42	(15-51)[f]	11.6	6.3	–23.6	–8.7	1.92
Transient	95	(48-91)[f]	49.2	12	–11.8	–3.1	3.58

[a] Estimations of DCM mass dissipation based on mass balance between inflow and outflow at z = 0.15 m.
[b] Extent of DCM degradation based on stable C isotopes observed at the inflow and outflow of the domain (z = 0.15 m) and according to κ-bacterial populations. For concomitant DCM degradation, two main competing pathways were considered for Dhbium and Diely (Eq. 11).
[c] Based on inflow and outflow observations (z = 0.15 m).
[d] According to Eq. 8.
[e] According to Eq. 10.
[f] A range of the extent of DCM degradation in laboratory aquifers was provided using reported ε_C and ε_{Cl} for both aerobic and anaerobic degradation pathways (Prieto-Espinoza et al., 2021).

The simulated changes in stable C and Cl isotope ratios of DCM according to distinct κ-bacterial populations (models C-E) were in accordance with initial ε_C and ε_{Cl} values associated with anaerobic DCM degradation. This confirmed a good model description of pathway-specific reaction rates (Tables 1 and 5). DCM degradation by Dhbium and Diely evidenced slight enrichment in ^{13}C and ^{37}Cl isotopes over time and according to distance from inflow compared to experimental results (SI, Section G). Nonetheless, models C-E underestimated DCM biodegradation by approximately 50% compared to experimental results (Table 5). This indicates that DCM biodegradation by a single simulated DCM-degrading

bacterial population is likely insufficient to capture the trends of DCM dissipation in the laboratory aquifers. The wide diversity of experimentally observed taxa potentially involved in DCM biodegradation further supports this result and justifies the need for model scenarios accounting for multiple bacterial metabolisms during DCM biodegradation.

The heterotrophic bacterial population B_{DOC} (X_4) showed a central role in regulating redox conditions and supporting DCM metabolism. B_{DOC} is capable of utilizing both O_2 and ferric iron as terminal electron acceptor during assimilation of DOC. Under steady-state, higher relative abundance of B_{DOC} was observed near the water table and across the CF for models C, D and E (Figure 3). Dissolved DOC was also established across the CF and followed similar concentration gradients as DCM (Figure 3). Hence, the constant supply of dissolved O_2 across the CF favored DOC mineralization resulting in an increase of B_{DOC} over time (Figure 3). The higher abundance of B_{DOC} across the CF can also be explained by its higher degradation rate during aerobic ($\mu_{max}^{BDOC,ox}$ = 1.0×10^{-5} [1/s]) than during anaerobic degradation ($\mu_{max}^{BDOC,anox}$ = 1.0×10^{-7} [1/s]) (Table 3), consistent with thermodynamic effects (Meckenstock et al., 2015). Similarly, the high abundance of Dhbium and Diely across the CF coincided with high CO_2 production by B_{DOC} (models D and E; Figure 3). Nevertheless, despite lower bacterial abundance of B_{DOC} across the SZ, dissolved Fe(III) (< 3 mg/L) and O_2 depletion (< 0.25 mg/L) were sufficient to maintain dissolved CO_2 concentrations across the SZ and thus to trigger DCM biodegradation by Dhbium and Diely across this zone (models D and E; Figure 3).

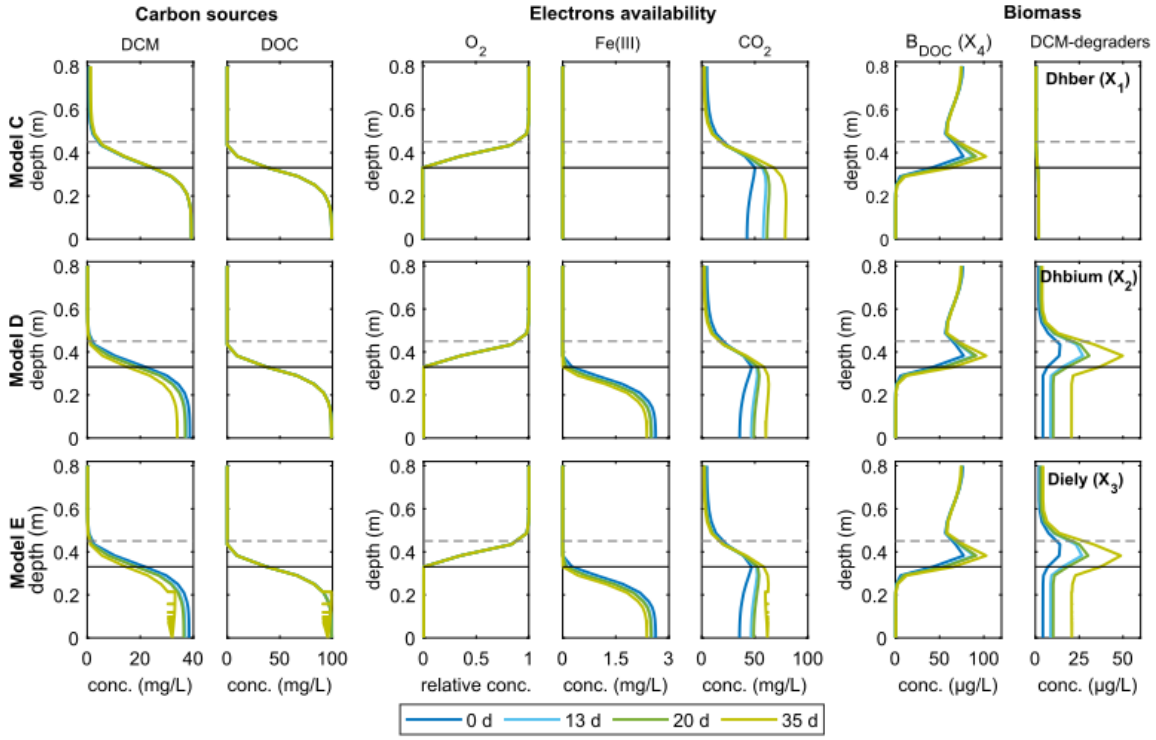

Figure 3. Carbon sources (DCM, DOC), redox species (O_2, Fe(III), CO_2) and biomass of four bacterial populations over time during simulations of DCM biodegradation by individual DCM degraders (Dhber, Dhbium and Diely in models C, D and E, respectively), and in the presence of heterotrophic groundwater bacteria (DOC assimilator B_{DOC}) under steady-state conditions. Horizontal lines represent the position of the water table (z = 0.33 m) and horizontal dashed lines represent the upper layer of the CF. Vertical profiles were retrieved at x = 0.65 m and at 0, 13, 20 and 35 days.

4.3 Concomitant DCM degradation by multiple bacterial populations under steady-state conditions

DCM biodegradation via multiple degradation pathways was tested accounting for active metabolism of Dhbium and Diely with and without the presence of Dhber, corresponding to models F and G, respectively (Table 4). The role of Dhber on DCM biodegradation was of interest as iron-reducing conditions prevailed in laboratory aquifers. Numerical simulations were also carried out in the presence of B_{DOC}. Overall, model simulations of concomitant DCM biodegradation under steady-state conditions (models F and G) evidenced larger DCM mass dissipation over time (simulated 43%; Figure 4) than simulations of metabolic activity by individual populations (Table 5). This agrees well with the experimentally observed DCM

574 dissipation (up to 42%; Table 5), and further supports the occurrence of multiple DCM
575 degradation pathways in laboratory aquifers. Comparisons between simulations in the absence
576 or presence of Dhber (models F and G, respectively) confirmed insignificant DCM degradation
577 under iron-reducing conditions (model G) compared to DCM fermentation or mineralization
578 (Figure 4 and Table 5). Iron-reducing conditions in the laboratory aquifers may thus be assigned
579 to the activity of heterotrophic bacteria not directly involved in DCM biodegradation.

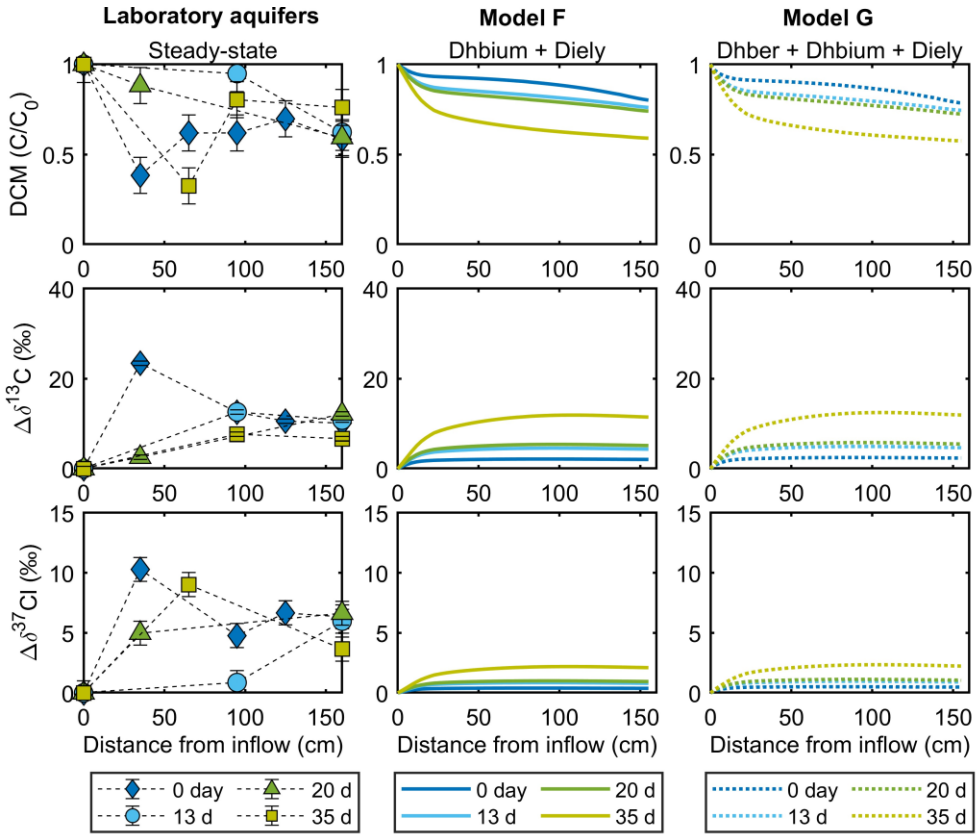

580

581 Figure 4. Concomitant DCM degradation by Dhber (X_1), Dhbium (X_2) and Diely (X_3) under
582 steady-state conditions (static water table) over time and distance from the aquifer inflow. From
583 left to right: measured data from the laboratory aquifers at z = 0.15 m (symbols), simulated
584 concomitant DCM degradation by Dhbium (X_2) and Diely (X_3) only (Model F), and simulated
585 concomitant DCM degradation by Dhber (X_1), Dhbium (X_2) and Diely (X_3) (Model G).
586 Heterotrophic groundwater bacteria B_{DOC} (X_4) was active in all models. From top to bottom:
587 DCM concentrations, evolution of C isotope fractionation ($\Delta\delta^{13}C$ in ‰), and evolution of Cl
588 isotope fractionation ($\Delta\delta^{37}Cl$ in ‰). All models had an incubation period of 60 days. The water
589 table was positioned at z = 0.33 m. Error bars are associated with DCM concentrations and
590 stable isotope values and represent standard errors with n = 3.

591

Simulated DCM removal during concomitant degradation by Dhber, Dhbium and Diely was accompanied by changes in C and Cl isotope ratios over time and with distance from inflow (Figure 4), with $\Delta\delta^{13}C$ of up to 12‰ and $\Delta\delta^{37}Cl$ of < 3‰ in the presence or absence of Dhber. In particular, changes in C isotope ratios followed the trends observed in laboratory aquifers ($\Delta\delta^{13}C$ of 12‰). This further supports the hypothesis that concomitant degradation of DCM likely occurred by multiple degradation pathways in the laboratory aquifers due to activity of a wide range of DCM degraders (Prieto-Espinoza et al., 2021). Dual plots of concomitant DCM degradation showed $\Lambda^{C/Cl}$ values distinct from those of individual κ-bacterial populations (Figure 5), thus reflecting the contribution of multiple DCM degradation pathways on overall DCM isotope signatures (Van Breukelen, 2007). The $\Lambda^{C/Cl}$ values computed from numerical simulations further indicated that bacterial populations Dhbium and Diely were the major contributors to DCM biodegradation. This was also supported by the increase of the transformation products acetate and formate over time (SI, Section H), which are the main transformation products during anaerobic DCM degradation by Dhbium and Diely (Chen et al., 2020). Overall, the similar $\Lambda^{C/Cl}$ values between models F and G confirmed the marginal role of Dhber during DCM biodegradation in model G (Table 5).

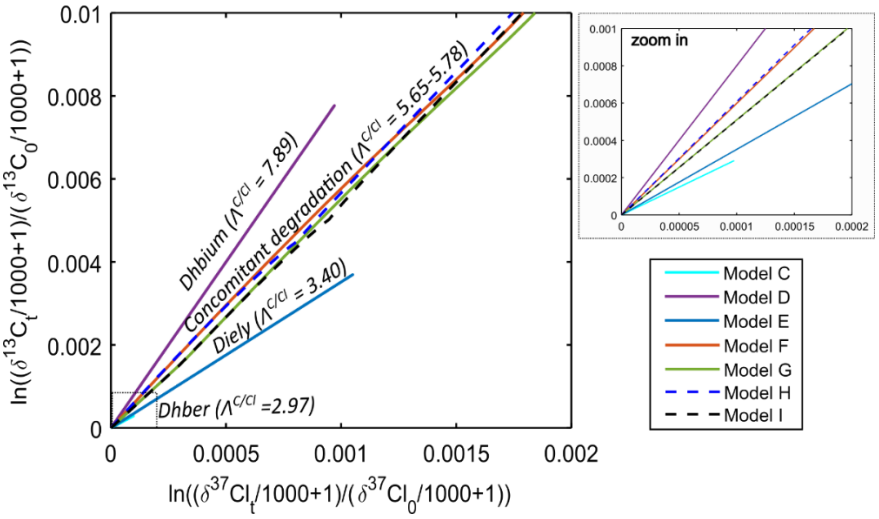

Figure 5. Simulated evolution of dual-element isotopes ($\Delta^{13}\delta C$ *versus* $\Delta^{37}\delta Cl$) during DCM biodegradation according to models C-I. Each line corresponds to simulations of distinct DCM degradation pathways by Dhber (model C), Dhbium (model D) and Diely (model E), as well as for concomitant DCM biodegradation by Dhbium and Diely under steady-state (model G) and transient (model I) conditions. Models F and H correspond to concomitant DCM biodegradation by Dhber, Dhbium and Diely under steady-state and transient conditions, respectively. For all modeled scenarios, heterotrophic groundwater bacteria B_{DOC} were present. Insert shows the low C and Cl isotope fractionation produced by Dhber due to limited metabolic activity during DCM biodegradation in the aquifer (model C).

4.4 Concomitant DCM degradation by multiple bacterial populations under transient conditions

Models H and I (i.e., in the presence and absence of Dhber, respectively) strongly suggested that biogeochemical dynamics created by water table fluctuations favor DCM removal in contaminated aquifers. Evolution of DCM concentrations and stable isotopes were followed in the SZ during water table fluctuation events (z = 0.15 m). Accordingly, the simulated mass removal of DCM was higher under transient flow conditions (95%) (upper panel; Figure 6) than under steady-state (43%) (upper panel; Figure 4). Numerical results of models H and I were consistent with experiments showing up to 95% DCM mass removal in laboratory aquifers (Table 5). Simulated DCM mass removal was also accompanied with an enrichment of ^{13}C and ^{37}Cl isotopes over time and distance from inflow (Figure 6). In models H and I, C isotope fractionation ($\Delta\delta^{13}C$) was up to 37‰ and 39‰, respectively, at the outlets

(x = 1.6 m) after 35 days, in agreement with experimental results (middle panel; Figure 6). Cl isotope fractionation resulted in $\Delta\delta^{37}Cl$ values of up to 7‰ (lower panel; Figure 6).

Simulated $\Lambda^{C/Cl}$ values during transient conditions showed similar values as those from steady-state conditions ($\Lambda^{C/Cl}$ range: 5.62-5.78) for all scenarios (models F-I; Figure 5). This indicated limitations of the numerical model to reproduce shifts in DCM biodegradation pathways triggered by water table fluctuations, as observed experimentally (steady state: $\Lambda^{C/Cl}$ = 1.92 *vs.* transient: $\Lambda^{C/Cl}$ = 3.52; Table 5). These limitations are likely associated with the proposed reactive framework in which κ-bacterial populations are mainly dependent on CO_2 availability (i.e., for Dhbium and Diely metabolism) produced by heterotrophic groundwater bacterial populations. Moreover, based on ME-CSIA data, the contribution of Dhbium and Diely on DCM degradation was 28% and 72%, respectively, for both flow regimes, and resulted in an overall extent of DCM degradation of approximately 35% and 80% under steady-state and transient conditions, respectively. These numerical results support the fact that closely related microorganism to Diely such as *Desulfosporosinus* sp. (Kleindienst et al., 2019) were likely implicated in DCM biodegradation under both flow regimes.

Numerical results also showed an increase in bacterial abundance across the fluctuation zone (z = 0.17-0.33 m; Figure 7). Under transient conditions, the observed increase of B_{DOC} across this zone was associated with O_2 diffusing deeper into the underlying groundwater during drainage events as shown in (abiotic) model B (Figure 2). This was beneficial for DOC assimilation by B_{DOC} upon oxygen respiration while maintaining O_2-depleted conditions during water table fluctuations (Figure 7). Overall, this supports that the dynamics of heterotrophic bacterial populations in laboratory aquifers likely controlled O_2 depletion during drainage and imbibition events (blue symbols; Figure 2). This was also coherent with the observed decrease in DOC with increasing distance from inflow in laboratory aquifers (Prieto-Espinoza et al., 2021). Moreover, approximately 80% of DCM was removed at the outlet after 13 days and

657 removal increased to up to 95% until the end of the experiment (model I; Figure 6),
658 corresponding to the first and second water fluctuation event, respectively.

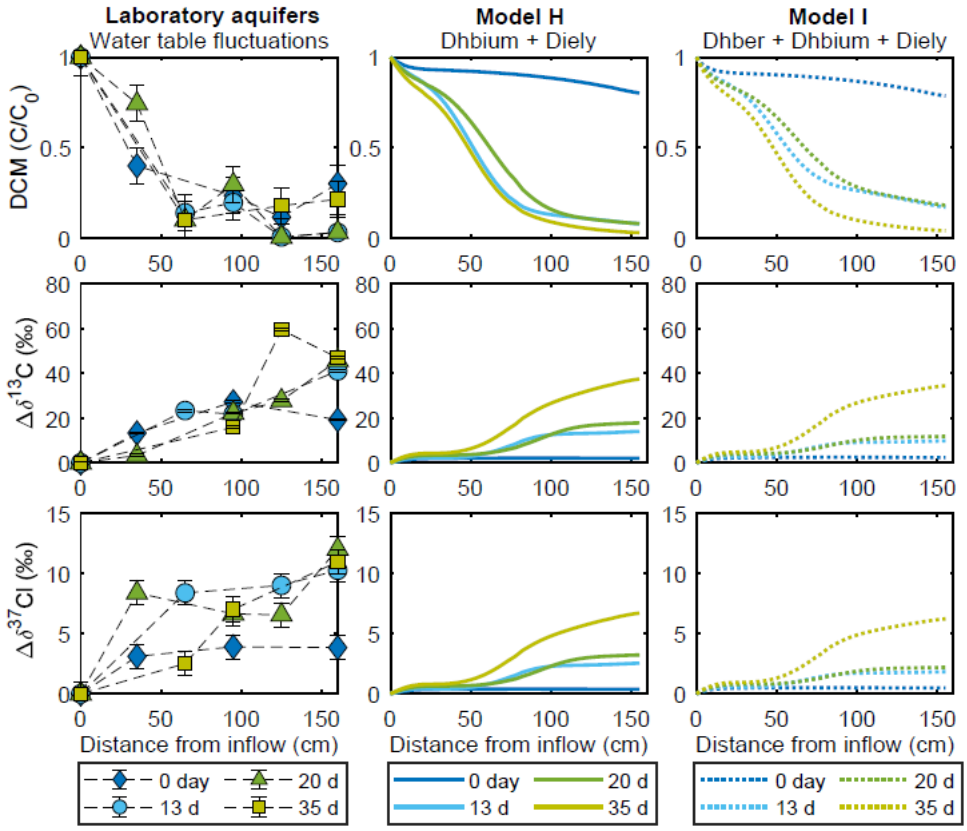

659

660 Figure 6. Concomitant DCM degradation by Dhber (X_1), Dhbium (X_2) and Diely (X_3) under
661 transient conditions (fluctuating water table) over time and distance from the aquifer inflow.
662 From left to right: measured data from the laboratory aquifers at z = 0.15 m (symbols), simulated
663 concomitant DCM degradation by Dhbium (X_2) and Diely (X_3) (Model H), and simulated
664 concomitant DCM degradation by Dhber (X_1), Dhbium (X_2) and Diely (X_3) (Model I).
665 Heterotrophic groundwater bacteria B_{DOC} (X_4) was active in all models. From top to bottom:
666 DCM concentrations, evolution of C isotope fractionation ($\Delta\delta^{13}C$ in ‰), and evolution of Cl
667 isotope fractionation ($\Delta\delta^{37}Cl$ in ‰). All models had an incubation period of 60 days. The water
668 table was positioned at z = 0.33 m and dropped to 0.17 m. For comparisons with experimental
669 results, model simulations follow the first water table fluctuation (corresponding to 0 to 13 d)
670 and the second water table fluctuation (corresponding to 20 to 35 d). Error bars are associated
671 with DCM concentrations and stable isotope values and represent standard errors with n = 3.

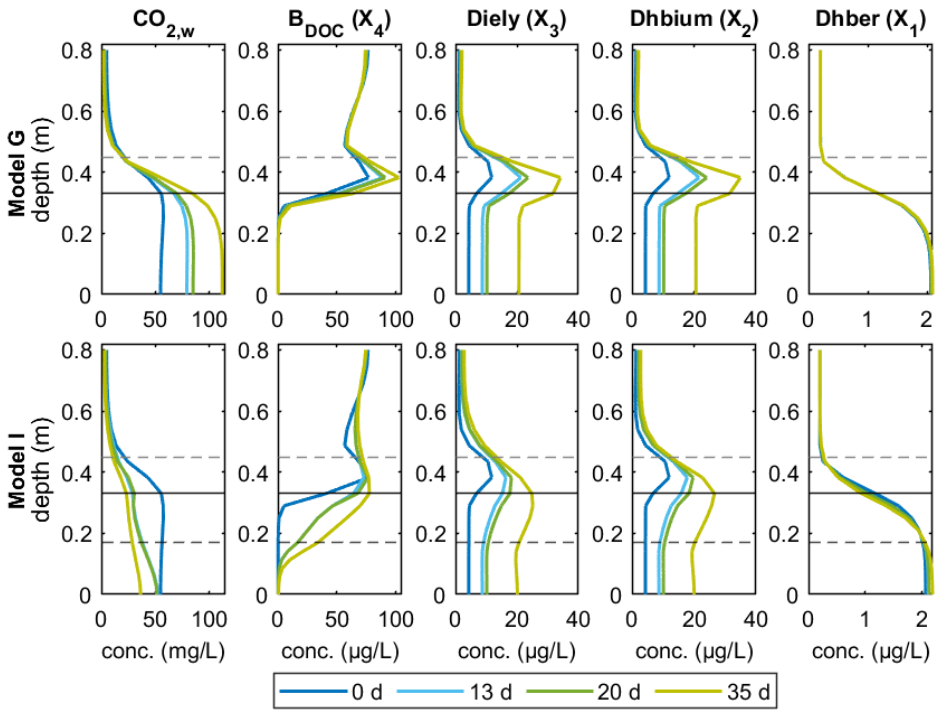

672

673 Figure 7. Change of CO_2 and active biomass concentrations over time during concomitant DCM
674 degradation by Dhber (X_1), Dhbium (X_2) and Diely (X_3) in the presence of the non-DCM
675 degrader B_{DOC} (X_4). Top: steady-state conditions (model G). Bottom: transient conditions
676 (model I). Horizontal lines represent the position of the water table (0.33 m from the bottom).
677 Upper dashed horizontal lines represent the upper limit of the CF. Lower dashed horizontal
678 lines represent the position of the water table after the fluctuation events (0.17 m from the
679 bottom). All depth profiles were retrieved at x = 0.65 m.

680

5. Discussion

This study demonstrates that previously obtained experimental results on bacterial DCM degradation, and in particular the intriguing impact of water table fluctuations, can indeed be modelled and confirmed numerically. Our work with contrasting abiotic and biotic scenarios show the key role of the capillary fringe on DCM biodegradation upon groundwater table fluctuations and highlight heterotrophic groundwater bacteria as key players. Further, only modelling scenarios taking redox conditions into account and in which multiple modes of DCM metabolism are present are compatible with experimental results, and highlight the added value of integrating CSIA data in RTMs .

5.1 The role of the capillary fringe in DCM biodegradation

In abiotic scenarios (models A and B), numerical simulations indicated that DCM volatilization across the CF was not a significant mechanism of DCM removal in laboratory aquifers under both flow regimes (Figure 2). Comparisons with biotic scenarios (models C-I) confirmed that DCM volatilization accounted for less than 10% and 16% under steady-state and transient conditions, respectively (Table 5), based on DCM aqueous concentrations and associated stable isotope fractionation. The steep water saturation levels formed across the CF restricted mass exchange of DCM due to low diffusion in water compared to the gas-phase (Jeannottat & Hunkeler, 2013). Under transient conditions, however, DCM volatilization across the fluctuation zone (z = 0.17-0.33 m) was suggested during drainage events (model B; Figure 2f) as a result of the residual contaminated water exposed to the gas phase (McCarthy & Johnson 1993; Werner & Höhener, 2002).

Under transient conditions, model B exhibited rapid oxygenation of the SZ after drainage (z = 0.17 m; Figure 2b). This contradicts the O_2-depleted conditions observed in laboratory aquifers at a low water table (Prieto-Espinoza et al., 2021). Haberer et al., (2012) showed that reoxygenation of an underlaying anoxic groundwater is directly related to the speed

and magnitude of the water table drop driving advective O_2 fluxes in the vertical direction. However, comparisons between O_2 transport during water table fluctuations (model B) and experimental results of the laboratory aquifers suggest the likely presence of aerobic bacteria consuming dissolved O_2 in aquifers. We thus propose that heterotrophic groundwater bacteria across the CF contribute to limit O_2 during water table fluctuations, as suggested previously (Jost et al., 2015b) and evidenced in models H and I for transient conditions (SI, Section H).

5.2 Interplay of redox conditions and multiple groundwater bacterial populations on DCM biodegradation

Our numerical simulations highlighted the complex interplay of multiple bacterial populations on DCM biodegradation. Steady-state models C, D and E underestimated DCM degradation by either Dhber, Dhbium or Diely, respectively, compared to experimental results (Table 5). However, simulations of concomitant DCM degradation by Dhbium together with Diely and/or Dhber (models F and G) yielded better fits to experimental results (Figures 4 and 6). This strongly suggests that different bacterial populations with different pathways are simultaneously active in degrading DCM under both flow regimes. Thus, RTMs that account for multiple bacterial metabolisms associated with different populations may be better suited for accurate predictions of biodegradation in DCM-contaminated aquifers (Chen et al., 2017; Trueba-Santiso et al., 2020).

Moreover, inclusion of heterotrophic bacteria (B_{DOC}) in all models was important due to the role of such organisms in shaping redox conditions across the aquifer and regulating O_2-depleted conditions across the CF and near the water table (Figure 3 and SI, Section H). Indeed, previous studies conclusively showed the importance of such metabolism across the CF (Hron et al., 2015; Jost et al., 2015a, 2015b; Rezanezhad et al., 2014). Our results thus supports that multi-phase flow and mass exchange processes play a key role in shaping dynamic biogeochemical conditions and contaminant biodegradation across fluctuation zones.

731 Our modelling also demonstrated that heterotrophic groundwater bacteria affected DCM
732 biodegradation, particularly for pathways requiring CO_2 (Figures 3 and 7). In particular, an
733 increase in anaerobic DCM-degraders Dhbium and Diely across the CF was confirmed due to
734 available CO_2 produced by B_{DOC} upon DOC degradation (up to 50 mg/L; Figures 3 and 7)
735 compared to abiotic conditions (<0.5 mg/L; Figure 2). Nevertheless, simulated Dhbium and
736 Diely were present across this zone despite the presence of dissolved O_2 (> 1 mg/L; Figures 3),
737 contrasting their strictly anaerobic metabolism (Holliger et al., 1998; Mägli et al., 1996). O_2
738 tolerance for some anaerobic DCM degraders such as *Desulfosporosinus* strains and
739 *Desulfovibrio* spp. have been suggested (Agostino et al., 2020; Mardanov et al., 2016; Ramel
740 et al., 2015), despite limited experimental evidence (Lueders, 2017). This may enable their
741 establishment across moderately oxygenated niches such as the CF. In the future, implementing
742 O_2 inhibition terms and bacterial dormancy in RTMs may help more accurately predict the
743 establishment of anaerobic degrader niches across oxic/anoxic redox gradients near the water
744 table and CF (Eckert et al., 2015), and improve integrative RTMs for in-depth understanding of
745 DCM metabolism across oxic/anoxic redox gradients.

746 **5.3 Water table fluctuations enhance DCM degradation in laboratory aquifers**

747 Numerical results of DCM biodegradation by multiple κ-bacterial populations (models
748 H and I) showed that dispersive mixing driving biogeochemical dynamics is necessary to
749 enhance DCM biodegradation during water table fluctuations, and also that mutualistic
750 relationships among groundwater bacteria should no longer be overlooked. Indeed, models H
751 and I showed that DCM mass dissipation increased during water table fluctuations (Figure 6)
752 compared to steady-state conditions (models F and G; Figure 4). Here, downward O_2 diffusion
753 was key to sustain DCM degradation in the fluctuation zone due to interactions with
754 heterotrophic bacteria (B_{DOC}). Nevertheless, numerical results also showed that a single water
755 fluctuation event (from 0 to 13 days; Figure 6) is sufficient to produce a strong effect on DCM

biodegradation (80% at 13 d; x = 1.60 m). This resulted in a simulated increase of Dhbium and Diely by approximately 15% across this zone (Figures 7), enough to enhance DCM degradation.

Our model also showed that biomass, O_2 and CO_2 are key parameters to be measured to capture biogeochemical variations caused by water table fluctuations in relation to DCM degradation. In particular, future flow-through experiments with a high-resolution monitoring of CO_2 could help to shed light on the relevance of heterotrophic groundwater bacteria during DCM biodegradation. Moreover, direct competition experiments between known anaerobic DCM degraders requiring CO_2 such as Dhbium and Diely have not yet been reported. However, our model offers a flexible framework for corresponding processes during DCM degradation by such *Peptococcaceae* bacteria. It has recently been proposed that known anaerobic DCM degraders from the *Peptococcaceae* family share a unique anaerobic gene cassette, containing proteins *mecE* and *mecF* (for methylene chloride catabolism) (Murdoch et al., 2022). In the future, these genes may provide another line of evidence to monitor anaerobic DCM biodegradation in contaminated groundwater, and help further extend implementations of genome-scale metabolic RTMs (Scheibe et al., 2009).

It is worth stressing that high-resolution hydrochemical monitoring, ME-CSIA of DCM and biomolecular tools (16S rRNA gene) from the laboratory aquifers enabled the development of the reactive transport framework presented in this work. This framework underscored the interplay of redox conditions and several groundwater bacterial populations to enhance DCM biodegradation during water table fluctuations. In particular, the integration of stable isotopes of DCM (i.e., six isotopologues) in our multi-phase RTM proved useful to (i) quantify the biodegradation extent of DCM across different biotic scenarios and degradation pathways, and (ii) distinguish the effect of volatilization on the overall DCM mass dissipation.

An inverse modelling approach may further improve the applicability of our model to obtain a more suitable parametrization, particularly for bacterial-mediated processes. This could

be further extended to a sensitivity analysis on parameters related to bacterial kinetics, fundamental for appropriate descriptions of bacterial development during biodegradation reactions. Indeed, limitations of the dataset to test dissolved CO_2 and DCM transformation products (e.g., acetate and formate) were encountered, restricting in-depth interpretations of DCM biodegradation in the SZ and CF of the laboratory aquifers. Furthermore, anaerobic DCM degradation pathways and mechanisms are still poorly understood, which calls for future studies to elucidate the possibility of concomitant anaerobic DCM degradation at contaminated sites.

6. Conclusions

The proposed mathematical formalism describing multi-phase flow, multi-component and pathway-specific reaction rates of DCM proved suitable for shedding light on the multiple processes affecting reactive transport of DCM during water table fluctuations. In particular, the integration of ME-CSIA and pathway-specific reactions of four bacterial populations provided a reasonable understanding of the interplay between biogeochemical conditions and multiple bacterial metabolisms associated with DCM biodegradation under both steady-state and transient conditions. Most notably, only numerical simulations in which DCM biodegradation originated from multiple bacterial populations reproduced the DCM dynamics observed in laboratory aquifers. In addition, the contribution of heterotrophic groundwater bacteria (non-DCM degraders) on the overall DCM biodegradation was essential for providing CO_2 sources for fermentative pathways while maintaining O_2-depleted conditions across fluctuation zones. This highlights the importance of interactions within bacterial communities with regard to natural attenuation of DCM in contaminated groundwater, in contrast to the metabolic activity of a single bacterial population. The implemented model formalism with regard to DCM biodegradation highlights the added value of integrative RTMs in the evaluation of natural attenuation of DCM and other VOCs in contaminated groundwater.

Acknowledgments

M.P.E. was supported by a fellowship of the Ecole Nationale du Génie de l'Eau et de environment (ENGEES, France) and the doctoral school Earth and Environmental Sciences (ED 413) of the University of Strasbourg.

Author Contributions

Maria Prieto-Espinoza: Investigation, Conceptualization, Methodology, Software validation, Data curation, Visualization, Formal analysis, Writing - original draft, Writing - review & editing. Raphaël di Chiara-Roupert: Software, Investigation, Conceptualization, Methodology, Supervision, Writing - review & editing. Emilie E. L. Muller: Conceptualization, Writing – review & editing. Stéphane Vuilleumier: Conceptualization, Writing – review & editing. Sylvain Weill: Conceptualization, Funding acquisition, Resources, Supervision, Writing - review & editing. Gwenaël Imfeld: Conceptualization, Funding acquisition, Project administration, Resources, Supervision, Writing - review & editing.

Declaration of Competing Interests

The authors declare that they have no known competing financial interests or personal relationships that could have appeared to influence the work reported in this paper.

References

Agostino, V., Lenic, A., Bardi, B., Rizzotto, V., Phan, A. N. T., Blank, L. M., & Rosenbaum, M. M. (2020). Electrophysiology of the facultative autotrophic bacterium *Desulfosporosinus orientis*. Front. Bioeng. Biotechnol., 8:457. https://doi.org/10.3389/fbioe.2020.00457

Antelmi, M., Mazzon, P., Höhener, P., Marchesi, M., & Alberti, L. (2021). Evaluation of MNA in a chlorinated solvents-contaminated aquifer using reactive transport modeling coupled with isotopic fractionation analysis. Water, 13(21), 2945. https://doi.org/10.3390/w13212945

ATSDR, 2019. Substance Priority List. Retrieved: March 10, 2023 from https://www.atsdr.cdc.gov/spl/index.html.

Audí-Miró, C., Cretnik, S., Otero, N., Palau, J., Shouakar-Stash, O., Soler, A., & Elsner, M. (2013). Cl and C isotope analysis to assess the effectiveness of chlorinated ethene degradation by zero-valent iron: Evidence from dual element and product isotope values. Appl. Geochem., 32:175–183. https://doi.org/10.1016/j.apgeochem.2012.08.025

Badin, A., Braun, F., Halloran, L. J. S., Maillard, J., & Hunkeler, D. (2018). Modelling of C/Cl isotopic behaviour during chloroethene biotic reductive dechlorination: Capabilities and limitations of simplified and comprehensive models. Plos one, 13(8), p.e0202416. https://doi.org/10.1371/journal.pone.0202416

Barry, D. A., Prommer, H., Miller, C. T., Engesgaard, P., Brun, A., & Zheng, C. (2002). Modelling the fate of oxidisable organic contaminants in groundwater. *Advances in* Water Resources, *25*(8–12), 945–983. https://doi.org/10.1016/S0309-1708(02)00044-1

Blázquez-Pallí, N., Shouakar-Stash, O., Palau, J., Trueba-Santiso, A., Varias, J., Bosch, M., Soler, A., Vicent, T., Marco-Urrea, E., & Rosell, M. (2019a). Use of dual element isotope analysis and microcosm studies to determine the origin and potential anaerobic biodegradation of dichloromethane in two multi-contaminated aquifers. Sci. Total Environ., 696, 134066. https://doi.org/10.1016/j.scitotenv.2019.134066

Bouchard, D., Hunkeler, D., Gaganis, P., Aravena, R., Höhener, P., Broholm, M. M., & Kjeldsen, P. (2008). Carbon isotope fractionation during diffusion and biodegradation of petroleum hydrocarbons in the unsaturated zone: field experiment at Værløse airbase, Denmark, and modeling. Environ. Sci. Technol., 42(2), 596–601. https://doi.org/10.1021/es070718f

Brooks, R. H., & Corey, T. A. (1965). Hydraulic properties of porous media. Hydrology Paper No. 3, Civil Engineering Department, Colorado State University, Fort Collins, CO.

Brown, P. N., Hindmarsh, A. C., and Petzold, L. R. (1994). Using Krylov methods in the solution of large-scale differential-algebraic systems. SIAM J Sci. Comput., 15(6):1467–1488. https://doi.org/10.1137/0915088

Carrera, J., Saaltink, M. W., Soler-Sagarra, J., Wang, J., & Valhondo, C. (2022). Reactive transport: a review of basic concepts with emphasis on biochemical processes. Energies, 15(3), 925. https://doi.org/10.3390/en15030925

Chen, G., Fisch, A. R., Gibson, C. M., Erin Mack, E., Seger, E. S., Campagna, S. R., & Löffler, F. E. (2020). Mineralization versus fermentation: Evidence for two distinct anaerobic bacterial degradation pathways for dichloromethane. ISME J, 14(4), 959–970. https://doi.org/10.1038/s41396-019-0579-5

Chen, G., Shouakar-Stash, O., Phillips, E., Justicia-Leon, S. D., Gilevska, T., Sherwood Lollar, B., Mack, E. E., Seger, E. S., & Löffler, F. E. (2018). Dual carbon–chlorine isotope analysis indicates distinct anaerobic dichloromethane degradation pathways in two members of *Peptococcaceae*. Environ. Sci. Technol., 52(15), 8607–8616. https://doi.org/10.1021/acs.est.8b01583

Chen, G., Kleindienst, S., Griffiths, D. R., Mack, E. E., Seger, E. S., & Löffler, F. E. (2017). Mutualistic interaction between dichloromethane-and chloromethane-degrading bacteria in an anaerobic mixed culture. Environ. Microbiol., 19(11), 4784-4796. https://doi.org/10.1111/1462-2920.13945

Contois, D. E. (1959). Kinetics of bacterial growth: Relationship between population density and specific growth rate of continuous cultures. J. Gen. Microbiol., 21(1), 40–50. https://doi.org/10.1099/00221287-21-1-40

Coplen, T. B. (2011). Guidelines and recommended terms for expression of stable-isotope-ratio and gas-ratio measurement results. Rapid Commun. Mass Spectrom., 25(17), 2538–2560. https://doi.org/10.1002/rcm.5129

D'Affonseca, F. M., Prommer, H., Finkel, M., Blum, P., & Grathwohl, P. (2011). Modeling the long-term and transient evolution of biogeochemical and isotopic signatures in coal tar–contaminated aquifers. Water Resour. Res., 47(5), W05518. https://doi.org/10.1029/2010WR009108

Eckert, D., Kürzinger, P., Bauer, R., Griebler, C., & Cirpka, O. A. (2015). Fringe-controlled biodegradation under dynamic conditions: Quasi 2-D flow-through experiments and reactive-transport modeling. J. Contam. Hydrol., 172, 100–111. https://doi.org/10.1016/j.jconhyd.2014.11.003

Eckert, D., Rolle, M., & Cirpka, O. A. (2012). Numerical simulation of isotope fractionation in steady-state bioreactive transport controlled by transverse mixing. J. Contam. Hydrol., 140–141, 95–106. https://doi.org/10.1016/j.jconhyd.2012.08.010

Elsner, M. (2010). Stable isotope fractionation to investigate natural transformation mechanisms of organic contaminants: Principles, prospects and limitations. J. Environ. Monit., 12(11), 2005–2031. https://doi.org/10.1039/C0EM00277A

European Commission. (2013). Priority substances and certain other pollutants according to Annex II of Directive 2008/105/EC - Environment - European Commission.

Haberer, C. M., Rolle, M., Cirpka, O. A., & Grathwohl, P. (2012). Oxygen transfer in a fluctuating capillary fringe. Vadose Zone J., 11(3), vzj2011.0056. https://doi.org/10.2136/vzj2011.0056

Hermon, L., Denonfoux, J., Hellal, J., Joulian, C., Ferreira, S., Vuilleumier, S., & Imfeld, G. (2018). Dichloromethane biodegradation in multi-contaminated groundwater: Insights from biomolecular and compound-specific isotope analyses. Water Research, 142, 217–226. https://doi.org/10.1016/j.watres.2018.05.057

907 Höhener, P. (2016). Simulating stable carbon and chlorine isotope ratios in dissolved
908 chlorinated groundwater pollutants with BIOCHLOR-ISO. J. Contam. Hydrol., 195,
909 52–61. https://doi.org/10.1016/j.jconhyd.2016.11.002
910 Höhener, P., & Imfeld, G. (2020). Quantification of Lambda (Λ) in multi-elemental
911 compound-specific isotope analysis. Chemosphere, 267, 129232.
912 https://doi.org/10.1016/j.chemosphere.2020.129232.
913 Holland, S. I., Edwards, R. J., Ertan, H., Wong, Y. K., Russell, T. L., Deshpande, N. P.,
914 Manefield, M. J., & Lee, M. (2019). Whole genome sequencing of a novel,
915 dichloromethane-fermenting *Peptococcaceae* from an enrichment culture. PeerJ, 7,
916 e7775. https://doi.org/10.7717/peerj.7775
917 Holliger, C., Hahn, D., Harmsen, H., Ludwig, W., Schumacher, W., Tindall, B., Vazquez, F.,
918 Weiss, N., & Zehnder, A. J. B. (1998). *Dehalobacter restrictus* gen. nov. and sp. nov.,
919 a strictly anaerobic bacterium that reductively dechlorinates tetra- and trichloroethene
920 in an anaerobic respiration. Arch. Microbiol., 169(4), 313–321.
921 https://doi.org/10.1007/s002030050577
922 Hron, P., Jost, D., Bastian, P., Gallert, C., Winter, J., & Ippisch, O. (2015). Application of
923 reactive transport modelling to growth and transport of microorganisms in the
924 capillary fringe. Vadose Zone J., 14(5) : vzj2014.07.0092.
925 https://doi.org/10.2136/vzj2014.07.0092
926 Hunkeler, D., Van Breukelen, B. M., & Elsner, M. (2009). Modeling chlorine isotope trends
927 during sequential transformation of chlorinated ethenes. Environ. Sci. Technol.,
928 43(17), 6750–6756. https://doi.org/10.1021/es900579z
929 Jeannottat, S., & Hunkeler, D. (2013). Can soil gas VOCs be related to groundwater plumes
930 based on their isotope signature? Environ. Sci. Technol., 47(21), 12115–12122.
931 https://doi.org/10.1021/es4010703
932 Jin, B., Nijenhuis, I., & Rolle, M. (2018). Simulation of dual carbon–bromine stable isotope
933 fractionation during 1,2-dibromoethane degradation. Isot. Environ. Health Stud.,
934 54(4), 418–434. https://doi.org/10.1080/10256016.2018.1468759
935 Jost, D., Haberer, C. M., Grathwohl, P., Winter, J., & Gallert, C. (2015a). Oxygen transfer in a
936 fluctuating capillary fringe: Impact of microbial respiratory activity. Vadose Zone J.,
937 14(5), vzj2014.04.0039. https://doi.org/10.2136/vzj2014.04.0039
938 Jost, D., Winter, J., & Gallert, C. (2015b). Noninvasive quantification of green fluorescent
939 protein labeled *Escherichia coli* in a dynamic capillary fringe by fluorescence
940 intensity. Vadose Zone J., 14(5), vzj2014.03.0028.
941 https://doi.org/10.2136/vzj2014.03.0028
942 Kaufmann, R., Long, A., Bentley, H., & Davis, S. (1984). Natural chlorine isotope variations.
943 Nature, 309(5966), 338–340. https://doi.org/10.1038/309338a0
944 Kleindienst, S., Chourey, K., Chen, G., Murdoch, R. W., Higgins, S. A., Iyer, R., Campagna,
945 S. R., Mack, E. E., Seger, E. S., Hettich, R. L., & Löffler, F. E. (2019).
946 Proteogenomics reveals novel reductive dehalogenases and methyltransferases
947 expressed during anaerobic dichloromethane metabolism. Appl. Environ. Microbiol.,
948 85(6). https://doi.org/10.1128/AEM.02768-18
949 Kleindienst, S., Higgins, S. A., Tsementzi, D., Chen, G., Konstantinidis, K. T., Mack, E. E., &
950 Löffler, F. E. (2017). '*Candidatus* Dichloromethanomonas elyunquensis' gen. nov.,

sp. nov., a dichloromethane-degrading anaerobe of the *Peptococcaceae* family. Syst. Appl. Microbiol., 40(3), 150–159. https://doi.org/10.1016/j.syapm.2016.12.001

Kovárová-Kovar, K., & Egli, T. (1998). Growth kinetics of suspended microbial cells: From single-substrate-controlled growth to mixed-substrate kinetics. Microbiol. Mol. Biol. Rev., 62(3), 646–666. https://doi.org/10.1128/MMBR.62.3.646-666.1998

Kuder, T., Philp, R., Van Breukelen, B. M., Thoeument, H. A. A., & Vanderford, M. (2016). Integrated stable isotope – Reactive transport model approach for assessment of chlorinated solvent degradation. ESTCP Project ER-201029; Environmental Security and Technology Certification Program, Arlington, Virginia.

Lee, M., Low, A., Zemb, O., Koenig, J., Michaelsen, A., & Manefield, M. (2012). Complete chloroform dechlorination by organochlorine respiration and fermentation: Microbial chloroform metabolism. Environ. Microbiol., 14(4), 883–894. https://doi.org/10.1111/j.1462-2920.2011.02656.x

Lee, M., Wells, E., Wong, Y. K., Koenig, J., Adrian, L., Richnow, H. H., & Manefield, M. (2015). Relative contributions of *Dehalobacter* and zerovalent iron in the degradation of chlorinated methanes. Environ. Sci. Technol., 49(7), 4481–4489. https://doi.org/10.1021/es5052364

Lueders, T. (2017). The ecology of anaerobic degraders of BTEX hydrocarbons in aquifers. FEMS Microbiol. Ecol., 93(1), fiw220. https://doi.org/10.1093/femsec/fiw220

Mägli, A., Messmer, M., & Leisinger, T. (1998). Metabolism of dichloromethane by the strict anaerobe *Dehalobacterium formicoaceticum*. Appl. Environ. Microbiol., 64(2), 646–650. https://doi.org/10.1128/AEM.64.2.646-650.1998

Mägli, A., Wendt, M., & Leisinger, T. (1996). Isolation and characterization of *Dehalobacterium formicoaceticum* gen. nov. sp. nov., a strictly anaerobic bacterium utilizing dichloromethane as source of carbon and energy. Arch Microbiol, 166(2), 101–108. https://doi.org/10.1007/s002030050362

Mardanov, A. V., Panova, I. A., Beletsky, A. V., Avakyan, M. R., Kadnikov, V. V., Antsiferov, D. V., Banks, D., Frank, Y. A., Pimenov, N. V., Ravin, N. V., & Karnachuk, O. V. (2016). Genomic insights into a new acidophilic, copper-resistant *Desulfosporosinus* isolate from the oxidized tailings area of an abandoned gold mine. FEMS Microbiol. Ecol., 92(8), fiw111. https://doi.org/10.1093/femsec/fiw111

McCarthy, K. A., & Johnson, R. L. (1993). Transport of volatile organic compounds across the capillary fringe. Water Resour. Res. 29(6), 1675–1683. https://doi.org/10.1029/93WR00098

Meckenstock, R. U., Elsner, M., Griebler, C., Lueders, T., Stumpp, C., Aamand, J., Agathos, S. N., Albrechtsen, H.-J., Bastiaens, L., Bjerg, P. L., Boon, N., Dejonghe, W., Huang, W. E., Schmidt, S. I., Smolders, E., Sørensen, S. R., Springael, D., & van Breukelen, B. M. (2015). Biodegradation: Updating the concepts of control for microbial cleanup in contaminated aquifers. Environ. Sci. Technol., 49(12), 7073–7081. https://doi.org/10.1021/acs.est.5b00715

Meile, C., & Scheibe, T. D. (2019). Reactive transport modeling of microbial dynamics. Elements, 15(2), 111–116. https://doi.org/10.2138/gselements.15.2.111

Merlin, G., Thiebaud, H., Blake, G., Sembiring, S., & Alary, J. (1992). Mesocosms' and microcosms' utilization for ecotoxicity evaluation of dichloromethane, a chlorinated solvent. Chemosphere, 24(1), 37-50. https://doi.org/10.1016/0045-6535(92)90565-9

Michels, H. (1998). DISLIN manual. Max-Planck-Institut fur Aeronomie, Katlenburg-Lindau, 288. Retrieved: March 10, 2023 from http://www.dislin.de

Millington, R. J., & Quirk, J. P. (1961). Permeability of porous solids. Transactions of the Faraday Society, 57, 1200-1207.

Murdoch, R. W., Chen, G., Kara Murdoch, F., Mack, E. E., Villalobos Solis, M. I., Hettich, R. L., & Löffler, F. E. (2022). Identification and widespread environmental distribution of a gene cassette implicated in anaerobic dichloromethane degradation. Glob. Chang. Biol., 28(7), 2396-2412. https://doi.org/10.1111/gcb.16068

Ojeda, A. S., Phillips, E., & Sherwood Lollar, B. (2020). Multi-element (C, H, Cl, Br) stable isotope fractionation as a tool to investigate transformation processes for halogenated hydrocarbons. Environ. Sci.: Processes Impacts, 22(3), 567-582. https://doi.org/10.1039/C9EM00498J

Palau, J., Jamin, P., Badin, A., Vanhecke, N., Haerens, B., Brouyere, S., and Hunkeler, D. (2016). Use of dual carbon-chlorine isotope analysis to assess the degradation pathways of 1,1,1-trichloroethane in groundwater. Water Res., 92:235–243. https://doi.org/10.1016/j.watres.2016.01.057

Prieto-Espinoza, M., Di Chiara Roupert, R., Belfort, B., Weill, S., & Imfeld, G. (2023). Reactive transport of micropollutants in laboratory aquifers undergoing transient exposure periods. Sci. Total Environ., 856, 159170. https://doi.org/10.1016/j.scitotenv.2022.159170

Prieto-Espinoza, M., Weill, S., Belfort, B., Muller, E. E. L., Masbou, J., Lehmann, F., Vuilleumier, S., & Imfeld, G. (2021). Water table fluctuations affect dichloromethane biodegradation in lab-scale aquifers contaminated with organohalides. Water Res., 203, 117530. https://doi.org/10.1016/j.watres.2021.117530

Prommer, H., Anneser, B., Rolle, M., Einsiedl, F., & Griebler, C. (2009). Biogeochemical and isotopic gradients in a BTEX/PAH contaminant plume: Model-based interpretation of a high-resolution field data set. Environ. Sci. Technol., 43(21), 8206–8212. https://doi.org/10.1021/es901142a

Qt group. (2023). The Future of Digital Experiences. Retrieved: May 03, 2023 from https://www.qt.io/group

Ragsdale, S. W., & Pierce, E. (2008). Acetogenesis and the Wood–Ljungdahl pathway of CO_2 fixation. Biochim. Biophys. Acta - Proteins Proteom., 1784(12), 1873–1898. https://doi.org/10.1016/j.bbapap.2008.08.012

Ramel, F., Brasseur, G., Pieulle, L., Valette, O., Hirschler-Réa, A., Fardeau, M. L., & Dolla, A. (2015). Growth of the obligate anaerobe *Desulfovibrio vulgaris* hildenborough under continuous low oxygen concentration sparging: Impact of the membrane-bound oxygen reductases. *PLOS ONE*, *10*(4), e0123455. https://doi.org/10.1371/journal.pone.0123455

Renpenning, J., Keller, S., Cretnik, S., Shouakar-Stash, O., Elsner, M., Schubert, T., and Nijenhuis, I. (2014). Combined C and Cl isotope effects indicate differences between corrinoids and enzyme (*Sulfurospirillum multivorans* PceA) in reductive

dehalogenation of tetrachloroethene, but not trichloroethene. Environ. Sci. Technol., 48(20):11837–11845. https://doi.org/10.1021/es503306g

Rezanezhad, F., Couture, R.-M., Kovac, R., O'Connell, D., & Van Cappellen, P. (2014). Water table fluctuations and soil biogeochemistry: An experimental approach using an automated soil column system. J. Hydrol., 509, 245–256. https://doi.org/10.1016/j.jhydrol.2013.11.036

Rittmann, B. E. (2006). Microbial ecology to manage processes in environmental biotechnology. Trends Biotechnol., 24(6), 261–266. https://doi.org/10.1016/j.tibtech.2006.04.003

Rolle, M., Clement, T. P., Sethi, R., and Di Molfetta, A. (2008). A kinetic approach for simulating redox-controlled fringe and core biodegradation processes in groundwater: Model development and application to a landfill site in Piedmont, Italy. Hydrol. Process., 22(25):4905–4921. https://doi.org/10.1002/hyp.7113

Rühle, F. A., von Netzer, F., Lueders, T., & Stumpp, C. (2015). Response of transport parameters and sediment microbiota to water table fluctuations in laboratory columns. Vadose Zone J., 14(5):vzj2014.09.0116. https://doi.org/10.2136/vzj2014.09.0116

Scheibe, T. D., Mahadevan, R., Fang, Y., Garg, S., Long, P. E., & Lovley, D. R. (2009). Coupling a genome-scale metabolic model with a reactive transport model to describe *in situ* uranium bioremediation: Coupled genome-scale and reactive transport models. Microb. Biotechnol., 2(2), 274–286. https://doi.org/10.1111/j.1751-7915.2009.00087.x

Seybold, C. A., Mersie, W., Huang, J., & McNamee, C. (2002). Soil redox, pH, temperature, and water-table patterns of a freshwater tidal wetland. Wetlands, 22(1), 149–158. https://doi.org/10.1672/0277-5212(2002)022[0149:SRPTAW]2.0.CO;2

Trueba-Santiso, A., Fernández-Verdejo, D., Marco-Rius, I., Soder-Walz, J. M., Casabella, O., Vicent, T., & Marco-Urrea, E. (2020). Interspecies interaction and effect of co-contaminants in an anaerobic dichloromethane-degrading culture. Chemosphere, 240, 124877. https://doi.org/10.1016/j.chemosphere.2019.124877

Van Breukelen, B. M. (2007). Extending the Rayleigh equation to allow competing isotope fractionating pathways to improve quantification of biodegradation. Environ. Sci. Technol., 41(11), 4004–4010. https://doi.org/10.1021/es0628452

Weller, H. G., Tabor, G., Jasak, H., & Fureby, C. (1998). A tensorial approach to computational continuum mechanics using object-oriented techniques. Comput. Phys., 12(6):620–631. https://doi.org/10.1063/1.168744

Werner, D., & Höhener, P. (2002). The influence of water table fluctuations on the volatilization of contaminants from groundwater. Groundwater quality: Natural and enhanced restoration of groundwater pollution (Proceedings of the Groundwater Quality 2001 conference held at Sheffield, UK, June 2001. IAHS publication no. 275, 213–218.

Wiegert, C., Aeppli, C., Knowles, T., Holmstrand, H., Evershed, R., Pancost, R. D., Macháčková, J., & Gustafsson, O. (2012). Dual carbon-chlorine stable isotope investigation of sources and fate of chlorinated ethenes in contaminated groundwater. Environ. Sci. Technol., 46(20):10918–10925. https://doi.org/10.1021/es3016843

Wright, J., Kirchner, V., Bernard, W., Ulrich, N., McLimans, C., Campa, M. F., Hazen, T., Macbeth, T., Marabello, D., McDermott, J., Mackelprang, R., Roth, K., &

1081 Lamendella, R. (2017). Bacterial community dynamics in dichloromethane-
1082 contaminated groundwater undergoing natural attenuation. Front. Microbiol., 8, 2300.
1083 https://doi.org/10.3389/fmicb.2017.02300
1084 Zhang, Z. & Furman, A. (2021). Soil redox dynamics under dynamic hydrologic regimes – A
1085 review. Sci. Total Environ., 763:143026.
1086 https://doi.org/10.1016/j.scitotenv.2020.143026